

PROJECT REPORT

DEVELOPMENT OF EMPIRICAL FRAGILITY FUNCTIONS AFTER THE 2020
EARTHQUAKES IN AND AROUND TÜRKİYE

EEFIT Reseach Grant Scheme 2022
The Institution of Structural Engineers

Nurullah Acikgoz and Ufuk Hancilar
Kandilli Observatory and Research Institute
Department of Earthquake Engineering
Boğaziçi University

ABSTRACT

DEVELOPMENT OF EMPIRICAL FRAGILITY FUNCTIONS AFTER THE 2020 EARTHQUAKES IN AND AROUND TÜRKİYE

In 2020, two major earthquakes occurred that caused life losses and severe damages to the built environment in Türkiye: On January 24 an earthquake of moment magnitude 6.8 in the East Anatolian Fault Zone nearby Elazığ (Sivrice) province and, an earthquake of moment magnitude 6.6 on the North Samos Fault in the Aegean Sea offshore Izmir (Seferihisar) province on October 30.

Immediately following these devastating ground shakings, the Turkish Ministry of Environment, Urbanization and Climate Change conducted large-scale and detailed post-earthquake damage surveys in both regions. The observational damage data collected by the technical staff of the Ministry consisted of 92,800 structures in Elazığ and 213,776 structures in Izmir. This project aims to construct comprehensive empirical fragility functions from these two damage datasets by employing statistical methods. To examine the uncertainties, fragility curves are produced using different ground motion models and local soil information from different sources, and to consider these effects a ground motion model using a logic tree approach is proposed.

Fragility curves for reinforced concrete moment-resisting frame type structures and unreinforced masonry structures, which are the predominant typologies in Türkiye, are proposed with their confidence intervals. Comparisons with the fragility functions for similar structures available in the literature are provided.

TABLE OF CONTENTS

ABSTRACT	i
LIST OF FIGURES	iii
LIST OF TABLES	vii
LIST OF SYMBOLS	ix
LIST OF ACRONYMS/ABBREVIATIONS	x
1. INTRODUCTION	1
1.1. Objectives and Outline of the Project	1
2. OVERVIEW OF THE POST-EARTHQUAKE SURVEY DATA	2
2.1. Definition of Damage States	2
2.2. Classification of Structures	2
2.3. General Information about Building Inventory	3
3. DERIVATION OF EMPIRICAL FRAGILITY FUNCTIONS	13
3.1. Introduction	13
3.2. Methodology	13
3.3. Effect of Ground Motion Uncertainties on Fragility Curves: An Example of Masonry Structures	15
3.3.1. V_s30 Variability	16
3.3.2. Ground Motion Model Variability	16
3.3.3. Resulting Fragility Curves for Masonry Structures Considering Ef- fect of Ground Motion Uncertainty	18
3.4. Results	19
3.5. Comparison with Existing Fragility Curves	25
3.6. Conclusions	28
3.7. Acknowledgments	30
REFERENCES	31
APPENDIX A: FRAGILITY CURVE PARAMETERS	35

LIST OF FIGURES

Figure 2.1.	Spatial distribution of the number of structures shown over the district-based percentages for (a) Elazığ and (b) Izmir.	6
Figure 2.2.	Damage distributions of building inventory as per sub-provinces compiled from post-earthquake damage surveys after the (a) Sivrice-Elazığ (M_w 6.8) earthquake and (b) Seferihisar-Aegean Sea (M_w : 6.6) earthquake.	6
Figure 2.3.	Distribution and cumulative percentage (red line) of structures affected in (a) Elazığ and (b) Izmir.	8
Figure 2.4.	Damage states of structures by building class in (a) Elazığ and (b) Izmir.	8
Figure 2.5.	Number of unreinforced masonry structures in Elazığ by (a) number of stories, (b) year of construction. Red lines show cumulative percentage.	9
Figure 2.6.	Number of unreinforced masonry structures in Elazığ by damage states. Red lines show cumulative percentage of the structures.	9
Figure 2.7.	Damage states of unreinforced masonry structures in Elazığ by (a) year of construction, (b) number of stories.	9
Figure 2.8.	Number of reinforced concrete structures in Elazığ by (a) number of stories, (b) year of construction. Red lines show cumulative percentage.	10
Figure 2.9.	Number of reinforced concrete structures in Elazığ by damage states. Red lines show cumulative percentage of the structures.	10
Figure 2.10.	Damage states of reinforced concrete structures in Elazığ by (a) year of construction, (b) number of stories.	10
Figure 2.11.	Number of unreinforced masonry structures in Izmir by (a) number of stories, (b) year of construction. Red lines show cumulative percentage.	11
Figure 2.12.	Number of unreinforced masonry structures in Izmir by damage states. Red lines show cumulative percentage of the structures.	11

Figure 2.13.	Damage states of unreinforced masonry structures in Izmir by (a) year of construction, (b) number of stories.	11
Figure 2.14.	Number of reinforced concrete structures in Izmir by (a) number of stories, (b) year of construction. Red lines show cumulative percentage.	12
Figure 2.15.	Number of reinforced concrete structures in Izmir by damage states. Red lines show cumulative percentage of the structures.	12
Figure 2.16.	Damage states of reinforced concrete structures in Izmir by (a) year of construction, (b) number of stories.	12
Figure 3.1.	V_s30 distribution in Elazığ province derived from (a) geological information and (b) USGS based on the topographic slope.	16
Figure 3.2.	Distribution of PGV (cm/s) using V_s30 from (a) geological information and (b) USGS based on the topographic slope.	18
Figure 3.3.	Fragility curves for slight damage for masonry structures in Elazığ using V_s30 values from (a) USGS and (b) QTM maps.	18
Figure 3.4.	Fragility curves for extensive damage for masonry structures in Elazığ using V_s30 values from (a) USGS and (b) QTM maps.	19
Figure 3.5.	Fragility curves for complete damage for masonry structures in Elazığ using V_s30 values from (a) USGS and (b) QTM maps.	19
Figure 3.6.	Spatial distribution of (a) PGA (g) and (b) PGV (cm/s) for Sivrice-Elazığ earthquake.	20
Figure 3.7.	Comparison of PGA and PGV values from recording stations and considered logic tree model.	20
Figure 3.8.	Damage states of the unreinforced masonry structures in Elazığ by (a) PGA intervals, (b) PGV intervals.	21
Figure 3.9.	Damage states of the reinforced concrete structures in Elazığ by (a) PGA intervals, (b) PGV intervals.	21
Figure 3.10.	PGA-based fragility curves for unreinforced masonry structures (a) B211, (b) B212 and (c) B210 (pre-2000). The circles represent the observed damage.	22

Figure 3.11. PGV-based fragility curves for unreinforced masonry structures (a) B211, (b) B212 and (c) B210 (pre-2000). The circles represent the observed damage.	22
Figure 3.12. PGA-based fragility curves for reinforced concrete structures (a) B511, (b) B512 and (c) B510 (pre-2000). The circles represent the observed damage.	23
Figure 3.13. PGV-based fragility curves for reinforced concrete structures (a) B511, (b) B512 and (c) B510 (pre-2000). The circles represent the observed damage.	23
Figure 3.14. PGA-based fragility curves for reinforced concrete structures (a) B521, (b) B522 and (c) B520 (pre-2000). The circles represent the observed damage.	23
Figure 3.15. PGV-based fragility curves for reinforced concrete structures (a) B521, (b) B522 and (c) B520 (pre-2000). The circles represent the observed damage.	24
Figure 3.16. PGA-based fragility curves for reinforced concrete structures (a) B501, (b) B502 and (c) B500 (pre-2000). The circles represent the observed damage.	24
Figure 3.17. PGV-based fragility curves for reinforced concrete structures (a) B501, (b) B502 and (c) B500 (pre-2000). The circles represent the observed damage.	24
Figure 3.18. Comparison of the fragility curves for (a) 2-story, non-ductile RC MRF structures in SYNER-G project (dashed lines) with B511 building class (solid lines), (b) 5-story, non-ductile RC MRF structures in SYNER-G project with B521 building class and (c) 5-story, ductile RC MRF structures in SYNER-G project with B522 building class suggested in this study	26
Figure 3.19. Comparison of the fragility curves for (a) 3-story RC MRF structures in Akkar et al. (2005) (dashed lines) with B512 building class (solid lines) and (c) 5-story RC MRF structures in Akkar et al. (2005) with B522 building class suggested in this study	26

- Figure 3.20. Comparison of the fragility curves for (a) low-rise RC MRF structures in Erberik (2008, a) (dashed lines) with B510 building class (solid lines), (b) mid-rise RC MRF structures in Erberik (2008, a) with B520 building class and (c) unreinforced masonry structures in Erberik (2008, b) with B520 building class suggested in this study . 27
- Figure 3.21. Comparison of the fragility curves for (a) low-rise RC MRF structures in Gaudio et al. (2017) (dashed lines) with B510 building class (solid lines), (b) mid-rise RC MRF structures in Gaudio et al. (2017) with B520 building class and (c) low and mid-rise RC MRF structures in Gaudio et al. (2017) with B500 building class suggested in this study 27
- Figure 3.22. Comparison of the fragility curves for (a) CR-LFM-CDN-H2 building class in Crowley et al. (2021) (dashed lines) with B511 building class (solid lines), (b) CR-LFM-CDN-H6 building class in Crowley et al. (2021) with B512 building class and (c) CR-LFM-CDL-H6 building class in Crowley et al. (2021) with B522 building class suggested in this study 28

LIST OF TABLES

Table 2.1.	Building classification parameters and index numbers of building types.	3
Table 2.2.	Distribution of building inventory and number structures having moderate damage or above on sub-provinces of Elazığ.	4
Table 2.3.	Distribution of building inventory and number of structures having moderate damage or above on sub-provinces of Izmir.	5
Table 2.4.	Definition of building classes and the corresponding number of structures in Elazığ and Izmir provinces.	7
Table 3.1.	Considered ground motion models and corresponding contributions of the logic tree model.	17
Table A.1.	PGA-based fragility curve parameters for building class B211.	35
Table A.2.	PGA-based fragility curve parameters for building class B212.	35
Table A.3.	PGA-based fragility curve parameters for building class B210.	35
Table A.4.	PGV-based fragility curve parameters for building class B211.	36
Table A.5.	PGV-based fragility curve parameters for building class B212.	36
Table A.6.	PGV-based fragility curve parameters for building class B210.	36
Table A.7.	PGA-based fragility curve parameters for building class B511.	37
Table A.8.	PGA-based fragility curve parameters for building class B512.	37
Table A.9.	PGA-based fragility curve parameters for building class B510.	37
Table A.10.	PGV-based fragility curve parameters for building class B511.	38
Table A.11.	PGV-based fragility curve parameters for building class B512.	38
Table A.12.	PGV-based fragility curve parameters for building class B510.	38
Table A.13.	PGA-based fragility curve parameters for building class B521.	39

Table A.14. PGA-based fragility curve parameters for building class B522.	39
Table A.15. PGA-based fragility curve parameters for building class B520.	39
Table A.16. PGV-based fragility curve parameters for building class B521.	40
Table A.17. PGV-based fragility curve parameters for building class B522.	40
Table A.18. PGV-based fragility curve parameters for building class B520.	40
Table A.19. PGA-based fragility curve parameters for building class B501.	41
Table A.20. PGA-based fragility curve parameters for building class B502.	41
Table A.21. PGA-based fragility curve parameters for building class B500.	41
Table A.22. PGV-based fragility curve parameters for building class B501.	42
Table A.23. PGV-based fragility curve parameters for building class B502.	42
Table A.24. PGV-based fragility curve parameters for building class B500.	42

LIST OF SYMBOLS

M_w	Moment Magnitude
S_a	Spectral Acceleration
T_1	Period at 1 second
β	Standard deviation of $\ln(IM)$
θ	Median of the fragility function
$\Phi ()$	Standard normal cumulative distribution function

LIST OF ACRONYMS/ABBREVIATIONS

ATC	Applied Technology Council
DG	Damage Grade
ELER	Earthquake Loss Estimation Routine
EMS	European Macroseismic Scale
GMPM	Ground Motion Predictive Models
HC	High-Code
HR	High-Rise
HRC	Homogenized Reinforced Concrete Scale
IM	Intensity Measure
LC	Low-Code
LR	Low-Rise
MLE	Maximum Likelihood Estimation
MMI	Modified Mercalli Intensity
MR	Mid-Rise
NC	No-Code
PGA	Peak Ground Acceleration
PGD	Peak Ground Displacement
PGV	Peak Ground Velocity
QTM	Quaternary, Tertiary and Mesozoic
RC MRF	Reinforced Concrete Moment Resisting Frame
URM	Unreinforced Masonry
USGS	United States Geological Survey
UTC	Universal Time Coordinate

1. INTRODUCTION

1.1. Objectives and Outline of the Project

Building damages caused by earthquakes lead to human casualties, economic losses, and social problems. For this reason, earthquake risk assessment plays an important role in the disaster risk reduction processes of earthquake-prone regions. Procedures of earthquake risk assessment involve defining earthquake ground motion as intensity measures (such as PGA, PGV, MMI) and determining physical damage using fragility functions that offer damage likelihood conditioned on defined ground motion intensity levels [1].

Türkiye experienced two significant earthquakes in 2020 that caused extensive damage. The Sivrice-Elazığ earthquake, with a moment magnitude (Mw) of 6.8, occurred on January 24, 2020 (17:55 UTC) along the East Anatolian Fault Zone. Its depth is roughly 8 km, and its epicenter is at 38°36'N, 39°06'E, inside the Sivrice district. 41 people lost their lives, 1607 people were hospitalized with injuries, and 547 of the structures that were visible collapsed [2]. Western Türkiye and Eastern Greece were shaken by a catastrophic earthquake with a moment magnitude (Mw) of 6.6 less than a year later, on October 30, 2020 (11:51 UTC). Its epicenter is situated in the Aegean Sea, north of Samos Island, at a latitude of 37° 88' N and longitude of 26° 70' E, and its depth is 14.9 km. The incident left significant damage in its wake, as well as a tsunami that inundated some areas of Seferihisar (Türkiye). Six structures completely collapsed, causing 117 fatalities and 1035 injuries. 4% of the Izmir province's building inventory got damaged at different levels [3].

This project aims to generate empirical fragility curves for pre-dominant building typologies in Türkiye utilizing observed damage data sets collected after the 2020 Sivrice-Elazığ and Seferihisar-Aegean Sea earthquakes considering epistemic and aleatoric uncertainties. For this purpose, observational damage data consisting of 92,800 structures in Elazığ province and 213,776 structures in Izmir province by the Turkish Ministry of Environment, Urbanization and Climate Change are utilized. The structures are classified based on the type of lateral load-resisting system, number of floors and seismic design level. Fragility functions for the identified building typologies are derived by statistical processing using the maximum likelihood estimation (MLE) method of the damage data sets separately. The resulting fragility curves are presented along with the associated uncertainties and are compared to the existing fragilities for similar structures.

The fragility curves obtained within the scope of this study were compared both with the existing studies in the literature for Türkiye and with the fragility curves created after the earthquakes occurring in Europe in upcoming sections.

2. OVERVIEW OF THE POST-EARTHQUAKE SURVEY DATA

2.1. Definition of Damage States

In the field of seismic risk assessment, the evaluation of a building's performance can be determined by setting specific criteria known as limit states. These limit states serve as thresholds that distinguish various levels of damage, while the damage state refers to the actual conditions the building experiences.

Fragility curve derivation methods typically utilize a discrete damage scale. Empirical approaches employ the scale to gather post-earthquake damage data, while analytical approaches link the scale to the structural properties that define a building's limit state, such as inter-story drift capacity.

To define damage states there are several damage grade scales in literature. Table 2.1 displays a comparison of the commonly employed damage scales such as ATC-13 [4], EMS98 [5], HAZUS99 [6], homogenized reinforced concrete (HCR) [7] which are commonly used damage state definitions in fragility functions compiled from Rossetto and Elnashai [7].

Considering the damage assessment forms used in the field surveys conducted by the Ministry of Environment, Urbanization and Climate Change after disasters, it was deemed appropriate to use HAZUS99 damage scale. Therefore, fragility curves are created for 4 damage states: slight, moderate, extensive, and complete damage.

2.2. Classification of Structures

The building typology classification generally adopted depends on those characteristics which are expected to influence the earthquake performance of the structure. To achieve this aim, building classification systems typically consider various factors such as the building's age, height, occupancy type, appropriate structural design, and construction quality. These factors are important because they influence a building's ability to withstand ground shaking and other earthquake-related forces.

In this project, building inventory is classified by updating Istanbul province probable earthquake loss estimates project by Istanbul Metropolitan Municipality [8]. This classification method makes use of 3 different parameters, which are the structural system type (i), the number of stories (j), and the year of construction (k), and the building

types are called Bijk. Classification parameters and index numbers are given in Table 2.1.

Table 2.1. Building classification parameters and index numbers of building types.

Index	Structural System Type (i)	Number of Stories (j)	Year of Construction (k)
0	Disregarded	Disregarded	Disregarded
1	Wooden	1 - 4 Story (LR)	pre - 1980 (NC)
2	Unreinforced Masonry (URM)	5 - 8 Story (MR)	1980 - 2000 (LC)
3	Prefabricated	9 - 19 Story (HR)	2000 - 2019 (HC)
4	Steel Frame	>20 Story	post - 2019 (HC)
5	Reinforced concrete moment resisting frame (RC MRF)	-	-
6	Reinforced concrete shear wall (tunnel formwork system)	-	-
7	Reinforced concrete shear wall and frame	-	-
8	Reinforced concrete and steel composite	-	-

Selected year of construction intervals are determined according to the year of legislation of the seismic code in Türkiye. Thus, 4 different year intervals are determined as pre-1979 (structures assumed not to be designed earthquake resistant), 1980-2000 band (structures assumed to be designed according to the 1975 earthquake code), 2000-2019 band (structures assumed to be designed according to the 1998 code) and after 2019 (structures assumed to be designed according to the 2018 Turkish Seismic Code).

2.3. General Information about Building Inventory

Traditionally, post-earthquake surveys are made by government officials after catastrophic events. Afterward considered two damaging earthquakes in Türkiye, large-scale and detailed field observations were made by Ministry of Environment, Urbanization and Climate Change. As a result, 92,800 structures in Elazığ and 213,776 structures in Izmir were investigated in the scope of field surveys. Unfortunately, we had to remove most of the survey data from our dataset because of the lack of some necessary information (e.g., year of construction, number of stories, coordinate of the building). Even after this removal process, we have 19,662 structures in Elazığ province and 45,096 structures in Izmir province.

A dependable and comprehensive database requires a credible and detailed survey. It is essential to collect a substantial sample size (more than 100 structures) across various intensity measurement levels, encompassing different building classes. This allows for the creation of fragility or vulnerability curves. The sample should accurately represent the entire population of affected structures and should not solely consist of data from damaged structures. Furthermore, precise information about the location (longitude and latitude) of each building and the underlying soil is necessary. The classification of structures should include details about the construction material, structural system, height, and occupancy. These attributes are considered the minimum criteria for establishing a high-quality database. Additionally, a thorough explanation of the damage or loss should

be available, for example, using four or more different damage states to describe the damage [9]. Considering these definitions, the data we have after the filtering process mentioned above can be called high-quality since it is derived from a reliable and detailed survey that consists of damage state, construction year, number of stories, structural system, and geographical coordinate.

After post-earthquake damage assessment studies, structures defined as moderate, extensive, or complete damage levels cannot be usable immediately after an earthquake. The summation of moderate, extensive, and complete damage is an important value since it is a parameter that determines the need for emergency shelter after an earthquake [10]. Considering the damage states and resulting building inventory after filtering the data with necessary information, the distribution of building inventory and number of structures having moderate damage or above on sub-provinces of Elazığ and Izmir is given in Table 2.2. and 2.3, respectively.

Figure 2.1 illustrates the spatial distribution of building inventory and distribution of building inventory on sub-provinces as a percentage for Elazığ and Izmir provinces, respectively. As can be seen from Figure 2.1.a, the building inventory in Izmir is concentrated in Bayraklı and Bornova sub-provinces (approximately 55% of total surveyed structures). Figure 2.1.b shows that the majority (approximately 68%) of the structures surveyed in Elazığ are located in the central district of Elazığ.

Table 2.2. Distribution of building inventory and number structures having moderate damage or above on sub-provinces of Elazığ.

Sub-Province	Number of Structures	Structures Having Moderate Damage or Above
Merkez	13,440	2,860
Karakoçan	1,361	186
Kovancılar	1,229	305
Baskil	1,102	333
Palu	972	215
Sivrice	773	396
Maden	739	225
Keban	38	28
Arıcak	8	4
Ağın	0	0
Alacakaya	0	0
Total	19,662	4,552

Table 2.3. Distribution of building inventory and number of structures having moderate damage or above on sub-provinces of Izmir.

Sub-Province	Number of Structures	Structures Having Moderate Damage or Above
Bornova	14,302	29
Bayraklı	10,446	156
Karşıyaka	5,792	56
Buca	2,101	20
Karabağlar	1,927	25
Seferihisar	1,798	23
Konak	1,394	25
Çiğli	1,022	24
Aliağa	740	17
Menemen	645	17
Urla	625	7
Gaziemir	595	6
Menderes	551	16
Dikili	549	12
Torbali	535	21
Kiraz	393	10
Karaburun	324	0
Foça	234	13
Çeşme	218	9
Kemalpaşa	206	9
Balçova	198	1
Narlidere	175	4
Bergama	163	7
Güzelbahçe	74	1
Tire	65	2
Selçuk	11	1
Ödemiş	8	0
Beydağ	1	0
Kınık	0	0
Total	45,096	512

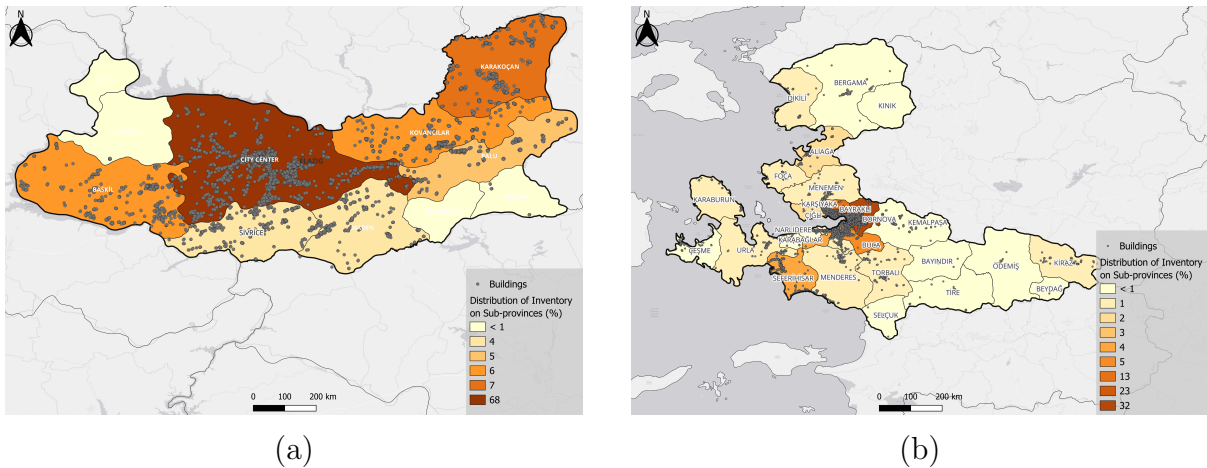


Figure 2.1. Spatial distribution of the number of structures shown over the district-based percentages for (a) Elazığ and (b) Izmir.

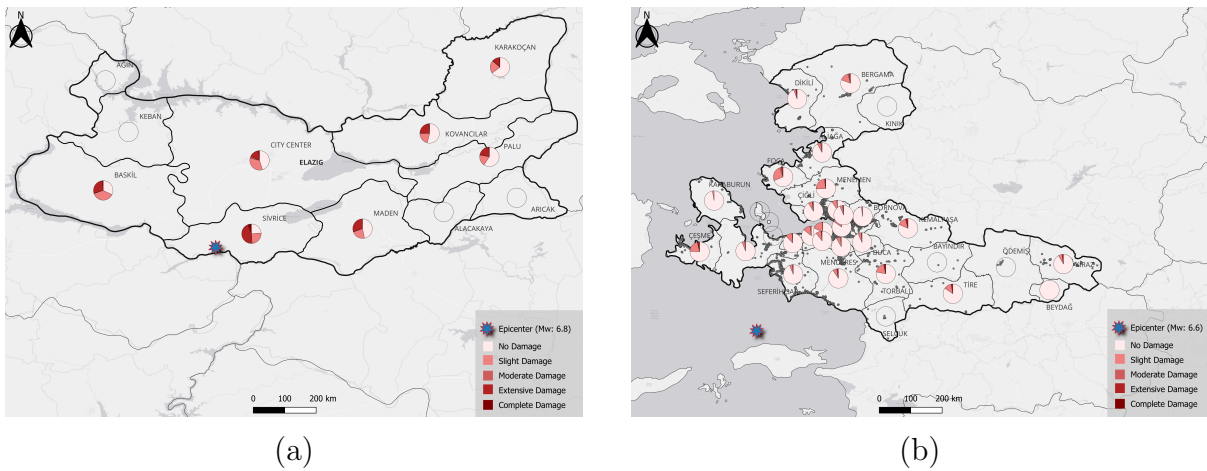


Figure 2.2. Damage distributions of building inventory as per sub-provinces compiled from post-earthquake damage surveys after the (a) Sivrice-Elazığ (M_w 6.8) earthquake and (b) Seferihisar-Aegean Sea (M_w : 6.6) earthquake.

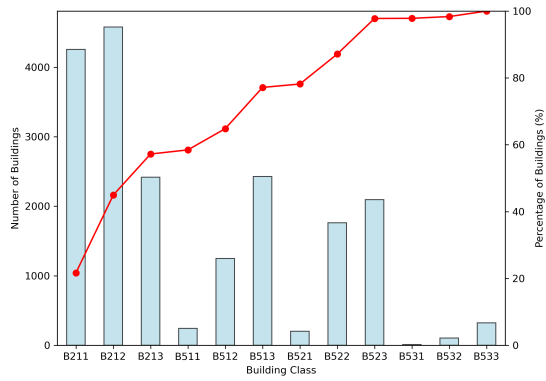
Figure 2.2 shows the resulting damage distributions of building inventory as per sub-provinces compiled from post-earthquake damage surveys after Sivrice-Elazığ (M_w : 6.8) and Seferihisar-Aegean Sea (M_w : 6.6) earthquakes. Figure 2.2.a shows that Sivrice district, which is closest to the epicenter of the earthquake, was the most damaged district in Elazığ. Significant damage is also observed in the central district. Figure 2.2.b shows that the damage rates are much lower in Izmir. The most damaged district in Izmir was Bayraklı district due to the ground conditions although it was far from the epicentre of the earthquake.

Table 2.4 shows the number of structures for each building class in Elazığ and Izmir provinces. Also, Figure 2.3 depicts the distribution and cumulative percentage of structures affected by Elazığ-Sivrice and Seferihisar-Aegean Sea earthquakes by building class. From Figure 2.3, it is seen that the ratio of masonry structures is high in the inventory affected by the Elazığ-Sivrice earthquake, while the ratio of reinforced concrete structures is high in the inventory affected by Seferihisar-Aegean Sea earthquake.

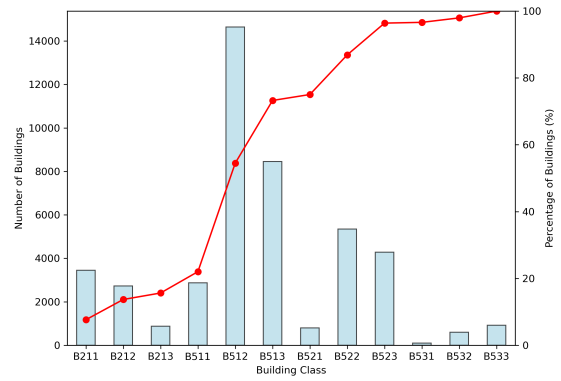
Table 2.4. Definition of building classes and the corresponding number of structures in Elazığ and Izmir provinces.

Building Class	Abbreviation	Elazığ Province	Izmir Province
B211	URM - LR - NC	4,256	3,445
B212	URM - LR - LC	4,579	2,733
B213	URM - LR - HC	2,417	874
B511	RC MRF - LR - NC	244	2,879
B512	RC MRF - LR - LC	1,248	14,645
B513	RC MRF - LR - HC	2,427	8,459
B521	RC MRF - MR - NC	200	802
B522	RC MRF - MR - LC	1,761	5,350
B523	RC MRF - MR - HC	2,095	4,286
B531	RC MRF - HR - NC	9	102
B532	RC MRF - HR - LC	104	602
B533	RC MRF - HR - HC	322	919
Total	-	19,662	45,096

In Figure 2.4, the damage states of structures by building class are illustrated for the structures affected by Elazığ-Sivrice and Seferihisar-Aegean Sea earthquakes. It can be seen that the level of damage in structures in Elazığ province is much more severe when compared to the structures in Izmir Province. Figures 2.5 to 2.16 provide further statistical information on the masonry and reinforced concrete structures in Elazığ and Izmir, such as the number of structures by number of stories, year of construction and damage states, percentage of damage states by year of construction and number of stories.

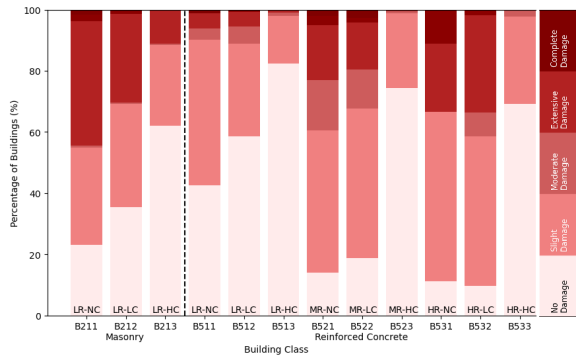


(a)

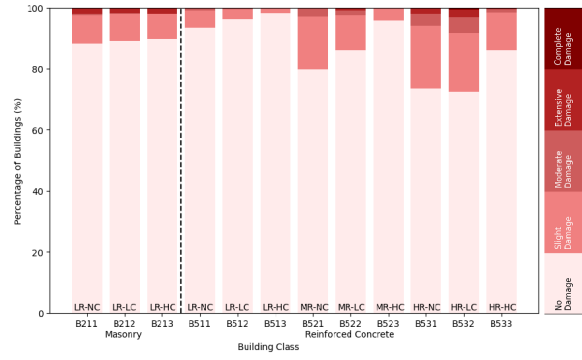


(b)

Figure 2.3. Distribution and cumulative percentage (red line) of structures affected in (a) Elazığ and (b) Izmir.



(a)



(b)

Figure 2.4. Damage states of structures by building class in (a) Elazığ and (b) Izmir.

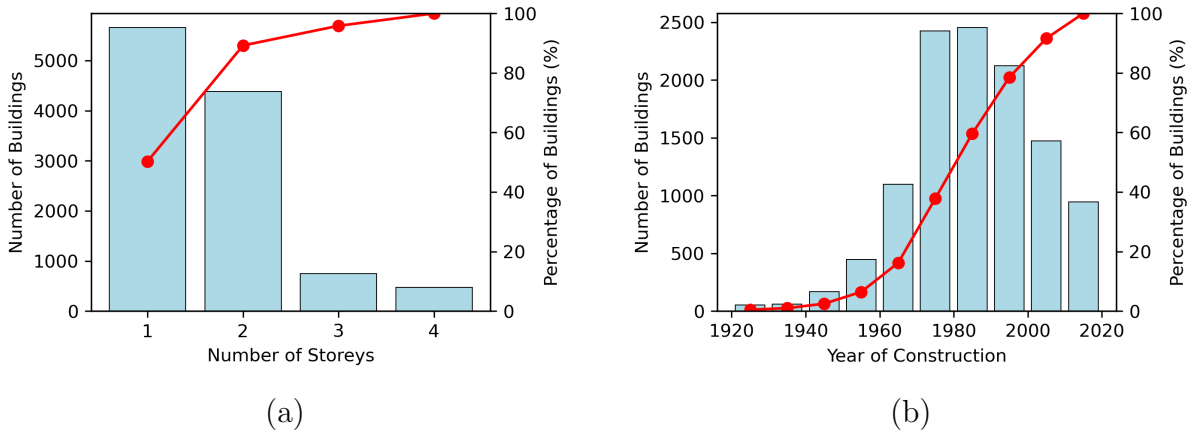


Figure 2.5. Number of unreinforced masonry structures in Elazığ by (a) number of stories, (b) year of construction. Red lines show cumulative percentage.

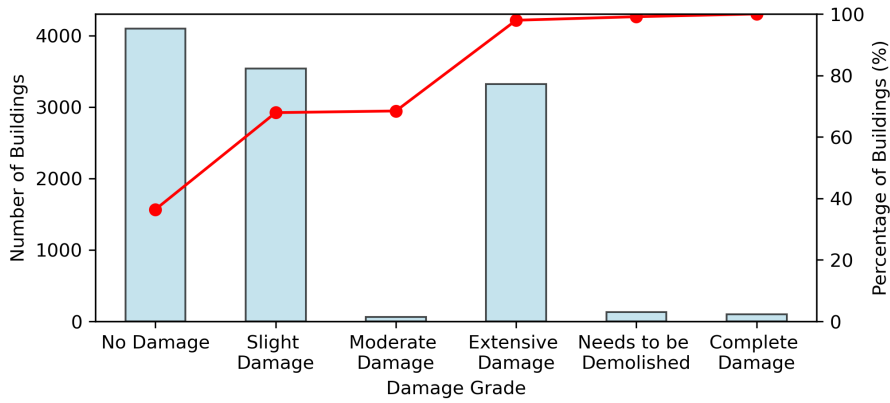


Figure 2.6. Number of unreinforced masonry structures in Elazığ by damage states. Red lines show cumulative percentage of the structures.

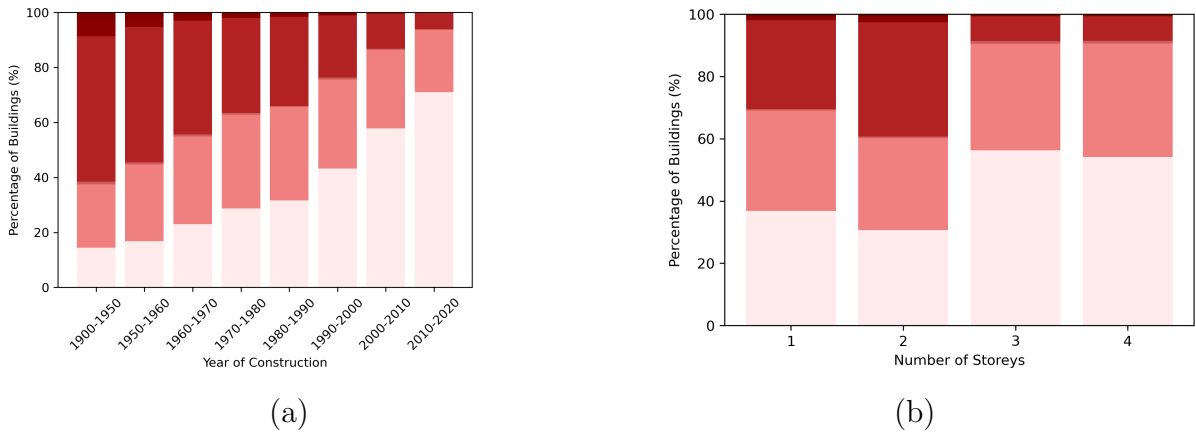


Figure 2.7. Damage states of unreinforced masonry structures in Elazığ by (a) year of construction, (b) number of stories.

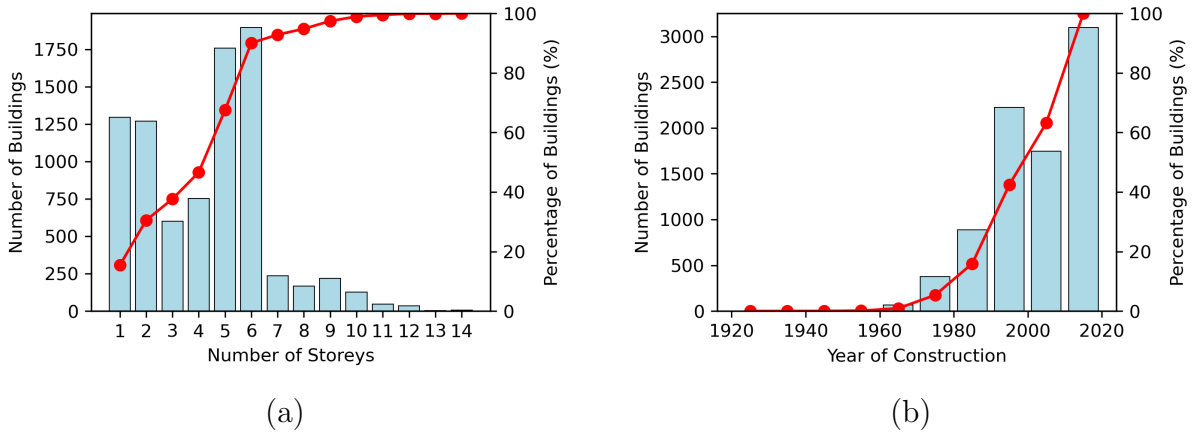


Figure 2.8. Number of reinforced concrete structures in Elazığ by (a) number of stories, (b) year of construction. Red lines show cumulative percentage.

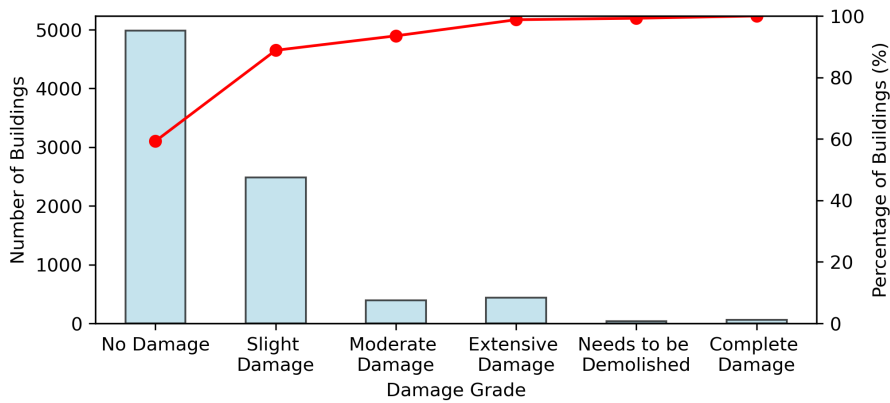


Figure 2.9. Number of reinforced concrete structures in Elazığ by damage states. Red lines show cumulative percentage of the structures.

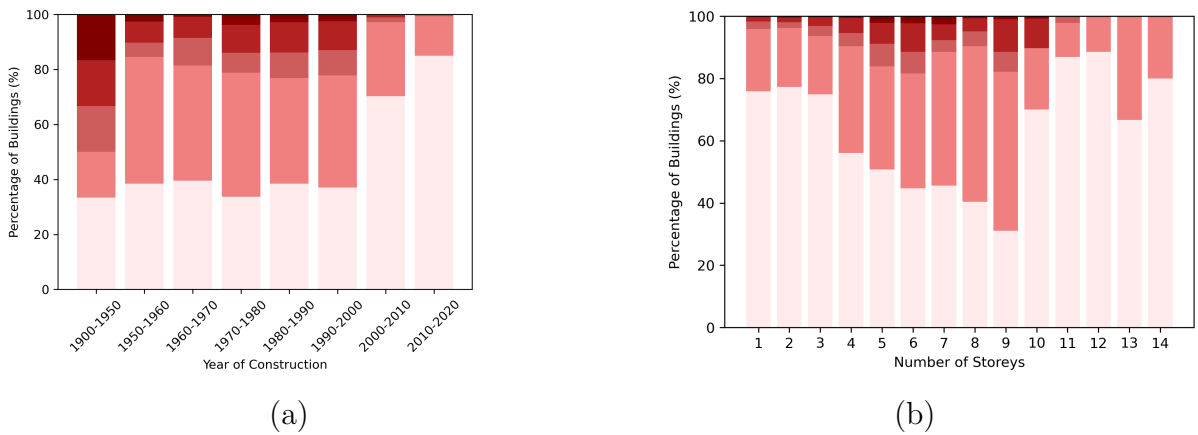


Figure 2.10. Damage states of reinforced concrete structures in Elazığ by (a) year of construction, (b) number of stories.

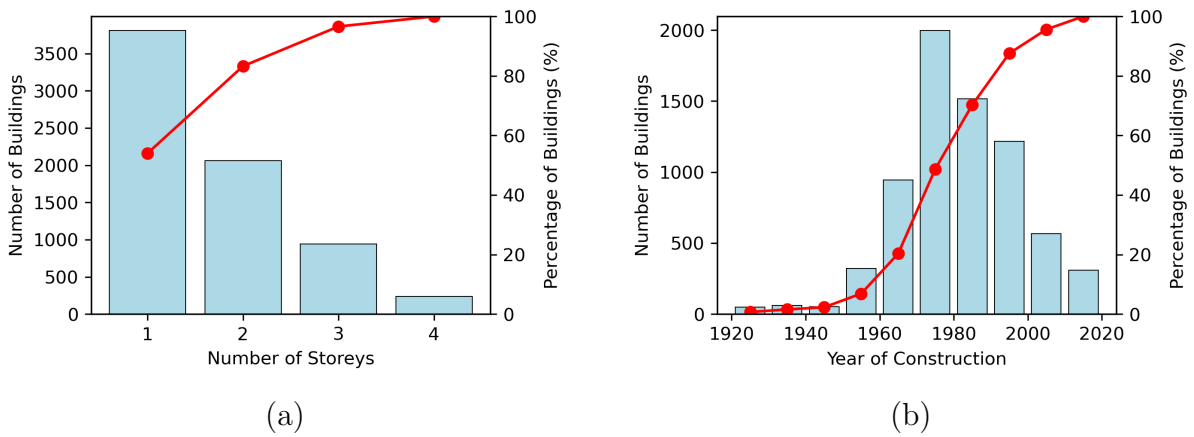


Figure 2.11. Number of unreinforced masonry structures in Izmir by (a) number of stories, (b) year of construction. Red lines show cumulative percentage.

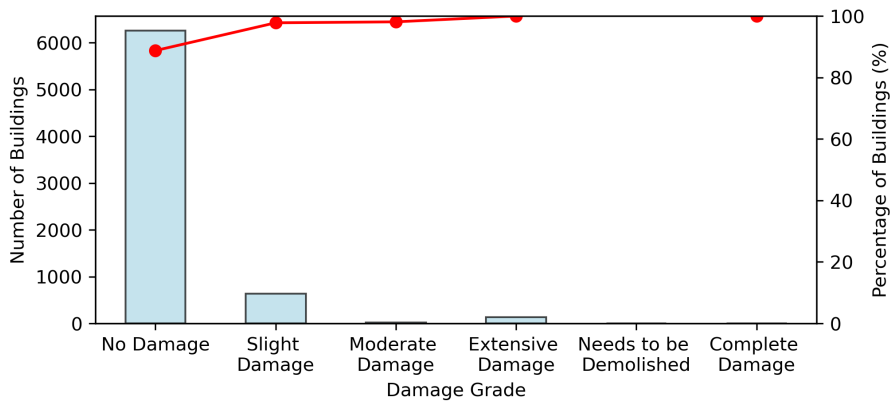


Figure 2.12. Number of unreinforced masonry structures in Izmir by damage states. Red lines show cumulative percentage of the structures.

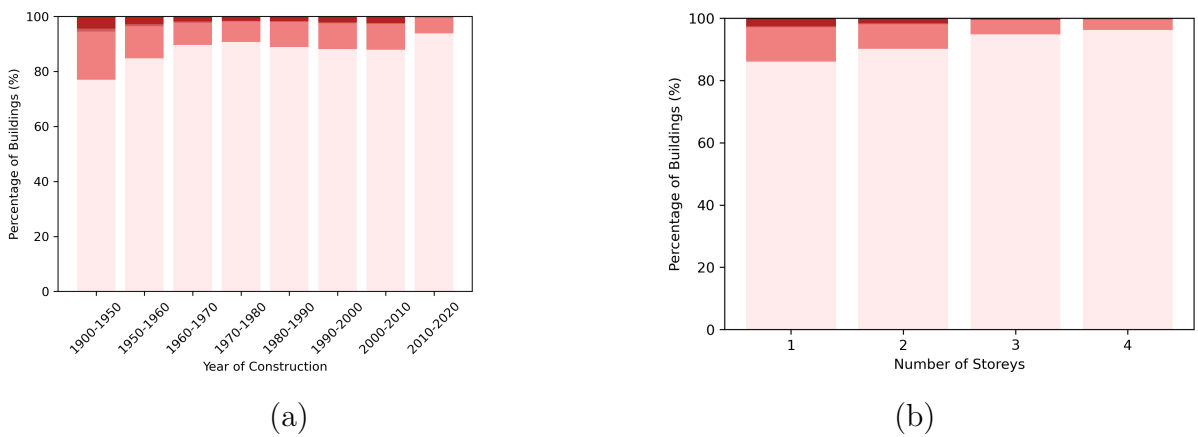


Figure 2.13. Damage states of unreinforced masonry structures in Izmir by (a) year of construction, (b) number of stories.

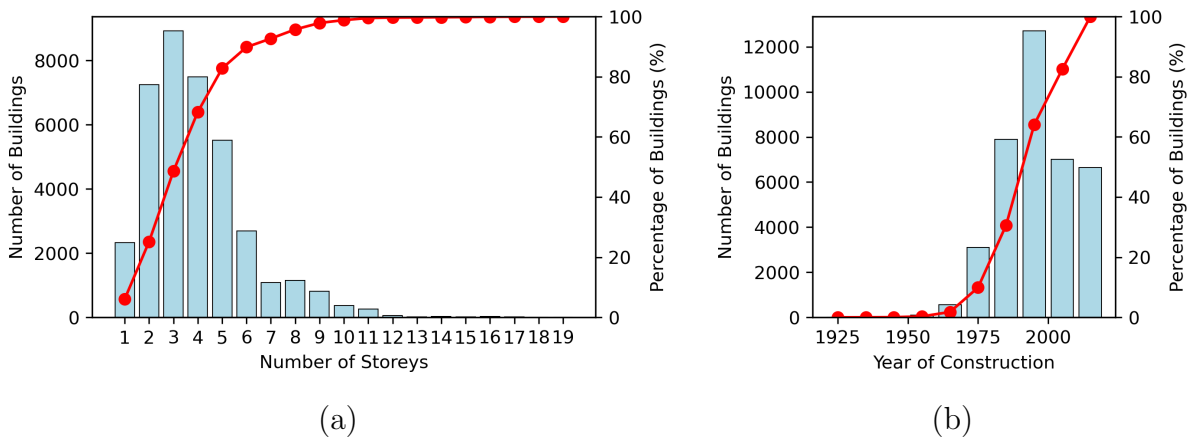


Figure 2.14. Number of reinforced concrete structures in Izmir by (a) number of stories, (b) year of construction. Red lines show cumulative percentage.

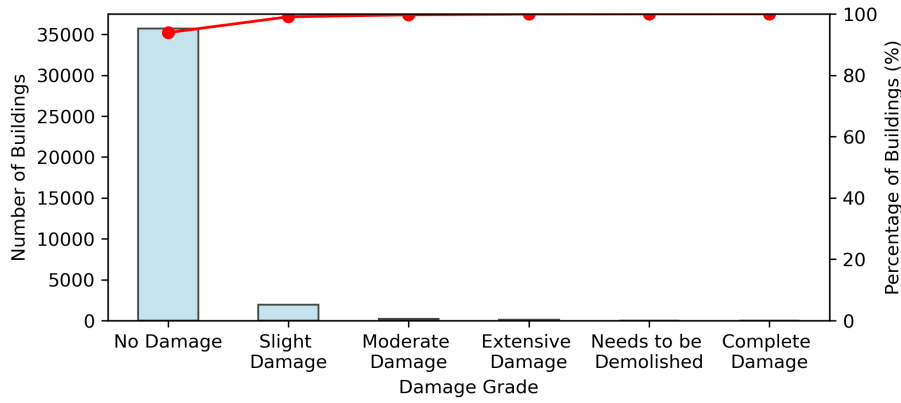


Figure 2.15. Number of reinforced concrete structures in Izmir by damage states. Red lines show cumulative percentage of the structures.

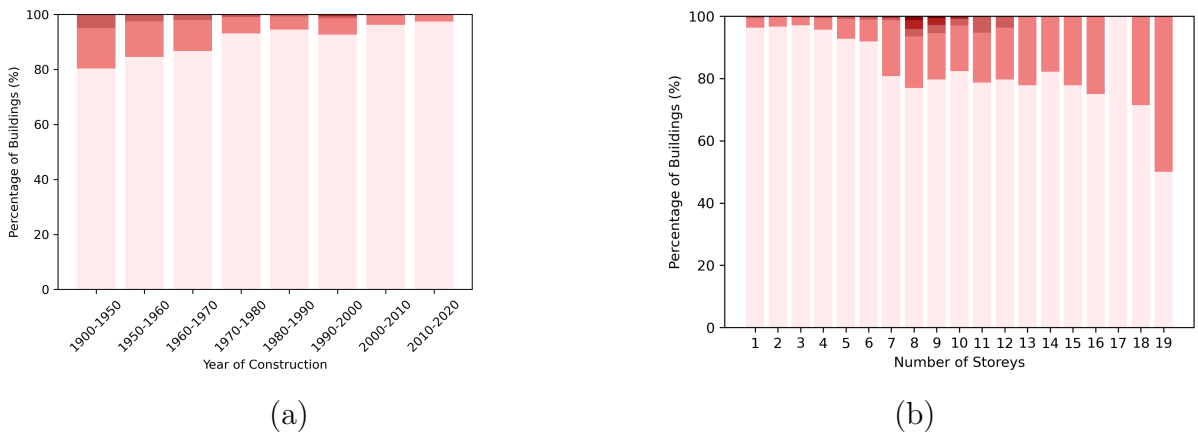


Figure 2.16. Damage states of reinforced concrete structures in Izmir by (a) year of construction, (b) number of stories.

3. DERIVATION OF EMPIRICAL FRAGILITY FUNCTIONS

3.1. Introduction

In this chapter, empirical fragility functions are derived for generic building classes described in the previous sections from the post-earthquake damage survey data from Sivrice-Elazığ (Mw: 6.8) and Seferihisar-Aegean Sea (Mw: 6.6) earthquakes. After explaining the methodology used to obtain the fragility functions, PGA and MMI-based fragility functions were obtained by using the earthquake ground motion maps provided by USGS and the inventories of Elazığ and Izmir. The functions obtained using USGS ground motion data can be considered as preliminary results. After the preliminary interpretation of these results, the effect of ground motion uncertainties and variabilities on the fragility functions was investigated. With the results obtained in this section, fragility functions were obtained for low and medium-rise structures constructed before 2000 by considering ground motion uncertainties. Finally, these fragility functions are compared with those in the literature.

3.2. Methodology

The main assumption to derive fragility functions in this study is that the cumulative standard lognormal distribution function is a suitable representation of earthquake damage distribution [11]. Fragility functions were calculated using the methodology offered Shinozuka et al. (2000) which utilizes the maximum likelihood estimation (MLE) method [12]. By examining the value of the parameter vector that maximizes the desired probability distribution, the maximum likelihood estimation principle seeks to identify the likelihood function that has the highest probability of producing the data already present in a dataset under consideration.

Baker (2015) explains the MLE method's process for analytical fragility functions [13]. Similar method is adapted for empirical fragility curves as follows. This study suggests that fragility functions are produced by applying a lognormal cumulative distribution function, which is given as

$$P(DG \mid IM = x) = \Phi\left(\frac{\ln(x/\theta)}{\beta}\right) \quad (3.1)$$

where $P(DG \mid IM = x)$ is the probability that a ground motion with $IM = x$ will cause the structure to exceed a specific DG, $\Phi(\cdot)$ is the standard normal cumulative distribution function, $\theta(\cdot)$ is the median of the fragility function and $\beta(\cdot)$ is the standard deviation of $\ln(IM)$ (can be called as the dispersion of IM).

The objective is to determine the best values for the fragility function's median and logarithmic standard deviation, respectively. The probability of observing z_j exceedance in n_j structures for a specific intensity measure level is obtained by the binomial distribution and can be expressed as

$$P(z_j \text{ exceedance in } n_j \text{ buildings in a class}) = \binom{n_j}{z_j} p_j^{z_j} (1 - p_j)^{n_j - z_j} \quad (3.2)$$

for a given IM level. In Equation 3.2, p_j is the probability of structures with $IM = x_j$ which exceeds a DG for a given building class that is defined in Equation 3.1. In this point, the greatest likelihood of p_j is given by the maximum likelihood approach.

When different intensity measure levels are used, the likelihood function, which is the product of the binomial probabilities (from Equation 3.2) at each intensity measure level can be written as

$$Likelihood = \prod_j^m \binom{n_j}{z_j} p_j^{z_j} (1 - p_j)^{n_j - z_j} \quad (3.3)$$

and if p_j is written in Equation 3.3, it is converted to

$$Likelihood = \prod_j^m \binom{n_j}{z_j} \Phi\left(\frac{\ln(x/\theta)}{\beta}\right)^{z_j} \left(1 - \Phi\left(\frac{\ln(x/\theta)}{\beta}\right)\right)^{n_j - z_j} \quad (3.4)$$

which describes the likelihood function. Since it is simpler to maximize a sum equation, Equation 3.4 is transformed into

$$\{\hat{\theta}, \hat{\beta}\} = \arg \max_{\theta, \beta} \sum_{j=1}^n \left\{ \ln \binom{n_j}{z_j} + \ln \Phi \left(\frac{\ln \left(\frac{x}{\theta} \right)}{\beta} \right) + (n_j - z_j) \ln \left(1 - \Phi \left(\frac{\ln \left(\frac{x}{\theta} \right)}{\beta} \right) \right) \right\} \quad (3.5)$$

by calculating the logarithm of both sides of Equation 3.4. In Equation 3.5, $\hat{\theta}$ and $\hat{\beta}$ are initial estimates of median and standard deviation.

All fragility curves derived in this study were obtained using this method. After this section, fragility curves were obtained using different ground motion inputs, sensitivity analyses were performed and confidence intervals were found for the obtained fragility curves.

3.3. Effect of Ground Motion Uncertainties on Fragility Curves: An Example of Masonry Structures

The process of obtaining empirical fragility curves involves many epistemic and aleatory uncertainties. In order to obtain empirical fragility curves, two basic information is needed: information about building's situation from post-earthquake damage surveys and the effect of the earthquake on the building which is determined by ground motion intensity measures.

There are uncertainties in the determination of the damage state of building, which is the first of these, such as the detail of the survey and the variability of the result according to the interpretation and damage discrimination ability of the person performing the survey.

In general, empirical fragility curve studies in the literature were built under the presumption that the ground intensity measure measurement error was minimal. However, the intensity levels are typically estimated using ground motion predictive models (GMPMs) or, more recently, ShakeMaps, due to the general lack of a dense strong-motion network in the areas of destructive earthquakes. Consequently, the ground motion intensity measurements are linked to high measurement error. Numerous studies that address this issue emphasize the significance of the impact of ground motion uncertainty and variabilities on fragility curves [14–18].

Different ground motion models and different V_s30 inputs are used to generate ground motion intensity measures to address effect on fragility curves and to obtain more consistent curves by using the logic tree method for different ground motion models. Ground motions are generated from ELER (The Earthquake Loss Estimation Routine) software [19] by using 5 different ground motion prediction equations. The V_s30 maps based on the topographic slope from USGS [20] and based on geological age information as Quaternary, Tertiary and Mesozoic (named as QTM after here) are used to define the soil class of the considered structures' location generated from General Directorate of Mineral Research and Exploration (MTA) of Türkiye.

3.3.1. V_s30 Variability

Ground motion values are calculated by using ELER (Earthquake Loss Estimation Routine) software. In ELER software there is a default V_s30 map which comes from USGS based on the topographic slope [20].

In addition, a different V_s30 map based on geological age information as Quaternary, Tertiary and Mesozoic (QTM) was introduced as an input to the ELER program for use in this study. Within the QTM map, the V_s30 velocity values for the Mesozoic (M) class are represented as 589 m/s, the Tertiary (T) class represented 406 m/s and the Quaternary (Q) class are represented as 333 m/s. Figures 3.21 and 2.22 illustrate the distribution of V_s30 values around Elazığ province based on QTM values and USGS topographic slope values, respectively.

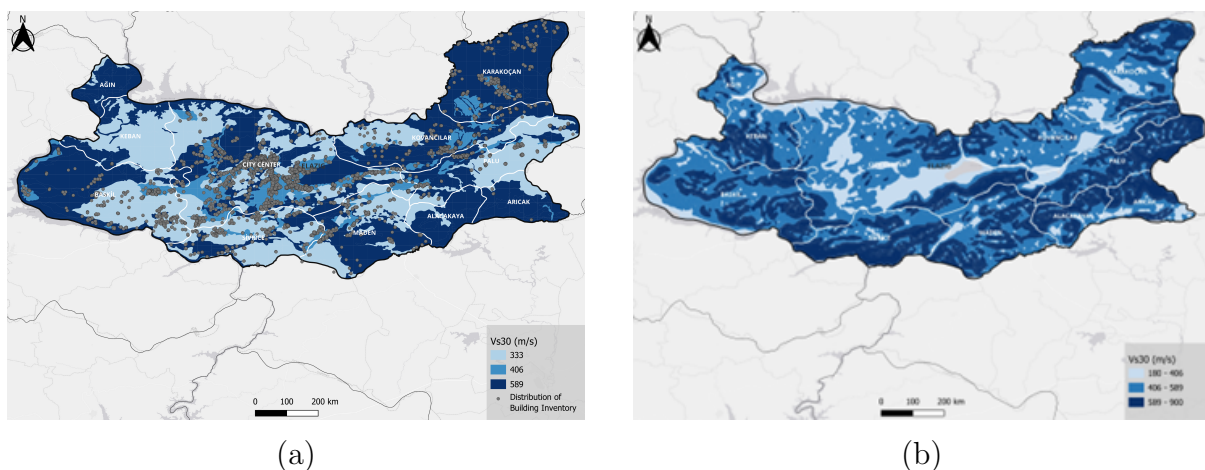


Figure 3.1. V_s30 distribution in Elazığ province derived from (a) geological information and (b) USGS based on the topographic slope.

3.3.2. Ground Motion Model Variability

For the vulnerability and fragility functions, as well as their confidence and prediction intervals, to be accurately assessed, uncertainty must be incorporated into IM [15].

Table 3.1. Considered ground motion models and corresponding contributions of the logic tree model.

Ground Motion Model	Abbreviation	Weighting
Akcar et al. 2014	ASB14	0.2
Abrahamson et al. 2014	ASK14	0.2
Boore et al. 2014	BSSA14	0.2
Chiou and Youngs 2014	CY14	0.2
Kale et al. 2015	KAAH15	0.2
Logic Tree Model	LT	1

Several ground motion models were used in this study to reduce uncertainty and identify the fragility curve that produces the fitted fragility curve with the smallest confidence bounds, or the optimum fragility curve.

A current study by Kale et al. (2019) used a variety of ranking techniques to assess how well ground motion models predicted earthquake activity in tectonic regions using the Turkish Strong Motion Database [21]. The findings of the analysis suggested that the Chiou and Youngs (2014)'s global model [22], Türkiye (TR)-adjusted Boore and Atkinson (2008) model [23], and the local Kale et al. (2015) model have better predictive performances in comparison to other ground motion models.

Çetin et al. (2021) inspect the geotechnical aspects of the Sivrice-Elazığ earthquake, and they assume that Abrahamson et al. (2014) model is satisfactory for rupture distances greater than 10 kilometers [24, 25]. Another recent study [26] has indicated that the global Next Generation Attenuation West 2 (NGA-W2) models have performed admirably during recent earthquakes in Türkiye [25], [27–29]. Also, this study confirms that the most recent local ground motion model developed for Türkiye by Kale et al. (2015) has exhibited satisfactory performance on various subsets of the Turkish ground motion dataset.

As a result, five of the aforementioned models were selected and a logic tree was created with these models. Table 3.1 shows the selected ground motion models and corresponding logic tree weights. For simplicity, the same weight is assigned to all five ground motion models.

Figure 3.23 and 3.24 shows the PGV distribution using a logic tree model with V_s30 coming from USGS and QTM values, respectively. It can be seen that there is not much difference between the two maps.

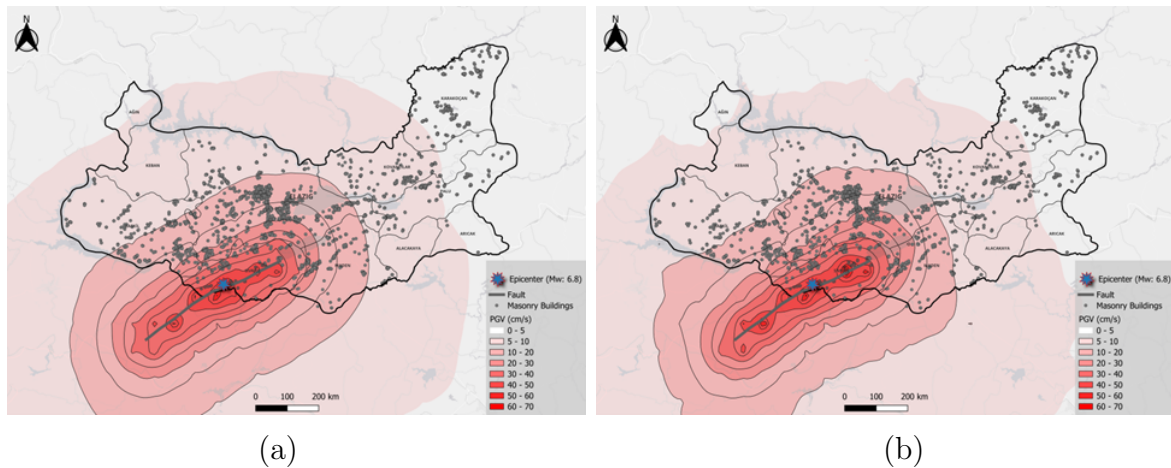


Figure 3.2. Distribution of PGV (cm/s) using V_s30 from (a) geological information and (b) USGS based on the topographic slope.

3.3.3. Resulting Fragility Curves for Masonry Structures Considering Effect of Ground Motion Uncertainty

To derive fragility curves, the same procedure explained in Chapter 3.2 was implied. Resulting fragility curves using 5 different ground motion models and logic tree models using V_s30 values from USGS and QTM maps for slight, extensive and complete damage can be seen in Figures 3.25 to 3.27, respectively.

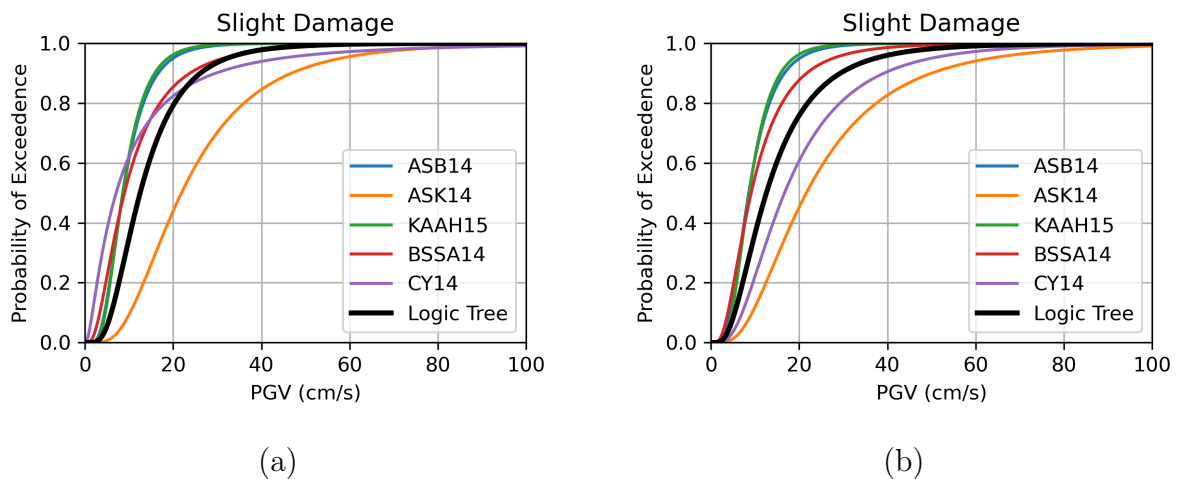


Figure 3.3. Fragility curves for slight damage for masonry structures in Elazığ using V_s30 values from (a) USGS and (b) QTM maps.

Fragility curves for all damage states illustrate that the use of different ground motion models resulted in noticeably different curves. As a recommendation, the study proposed adopting a logic tree approach to develop a ground motion model, rather than relying on a single model, to account for the epistemic uncertainties associated with ground motion models.

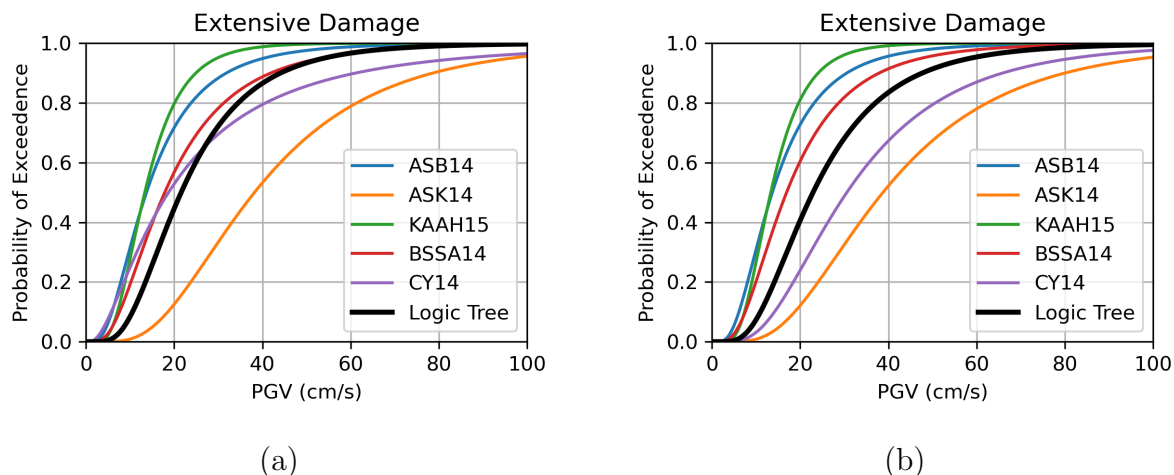


Figure 3.4. Fragility curves for extensive damage for masonry structures in Elazığ using V_{s30} values from (a) USGS and (b) QTM maps.

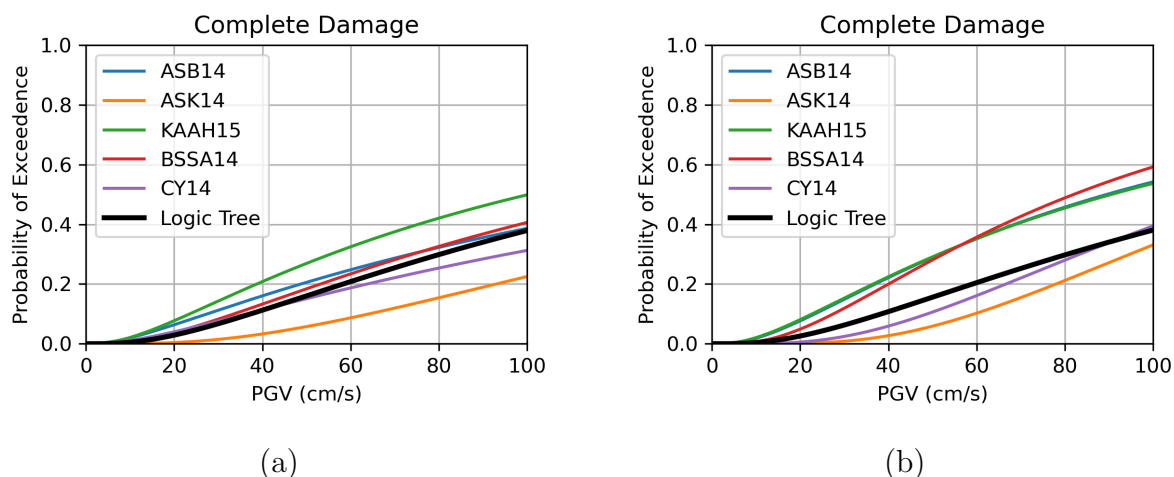


Figure 3.5. Fragility curves for complete damage for masonry structures in Elazığ using V_{s30} values from (a) USGS and (b) QTM maps.

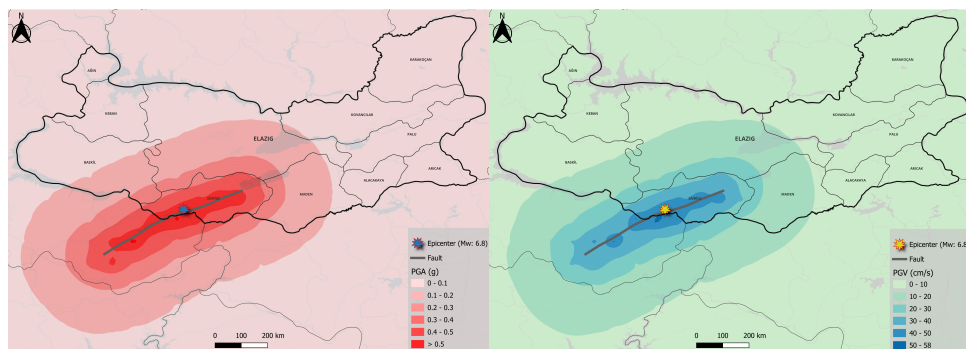
Moderate and extensive damage levels are very close to each other. This could be attributed to two main factors: inadequate design with insufficient engineering services or challenges faced by damage survey teams in accurately discerning between moderate and extensive damage. This limitation represents a significant drawback of the available data.

3.4. Results

According to the results obtained in the previous section, a fragility curve set was created by using the logic tree model and Elazığ building inventory to consider the uncertainties from different ground motion models. In empirical fragility studies, PGA, PGV and PGD are frequently used ground motion intensity measures. It is generally suggested that PGV and PGD are more associated to damage when they compared to

PGA. Contrarily, they are highly sensible to the amount of noise in record and the process of filtering. Additionally, there are fewer ground motion model for PGV and PGD than for PGA [30]. Considering this information, PGV was used in the development of fragility curves in addition to PGA, which is the most commonly used intensity measure. Figures 3.29 and 3.30 show the PGA and PGV distribution maps created with the logic tree model using V_s30 from QTM values. Also, Figure 3.31 illustrates the comparison of PGA and PGV values from recording stations and the considered logic tree model.

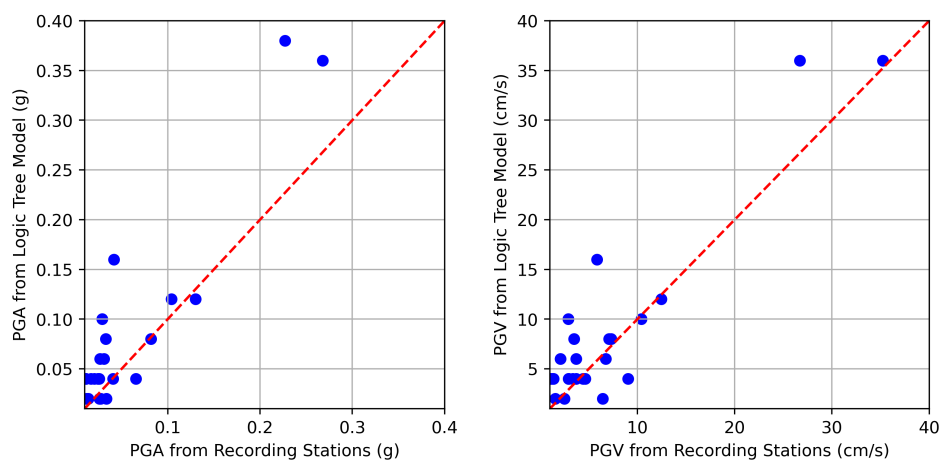
In this section, only the survey data obtained after the Sivrice-Elazığ earthquake is used since the damage rates are very low in the building inventory in Izmir province. In addition, the fragility curves produced in Section 3.3 showed that unreasonable results emerged due to the low damage rate in the structures built after 2000 and the low amount of data in the high-rise building classes. Therefore, fragility curves are obtained for low and medium-rise masonry and reinforced concrete structures constructed before 2000 by considering ground motion uncertainty.



(a)

(b)

Figure 3.6. Spatial distribution of (a) PGA (g) and (b) PGV (cm/s) for Sivrice-Elazığ earthquake.



(a)

(b)

Figure 3.7. Comparison of PGA and PGV values from recording stations and considered logic tree model.

Ground motion intensities are ranging from 0.1 to 0.6 (g) in PGA and 10 to 60 (cm/s) in PGV. Figures 3.32 and 3.33 illustrate the damage states by PGA intervals, and PGV intervals for unreinforced masonry and reinforced concrete structures, respectively.

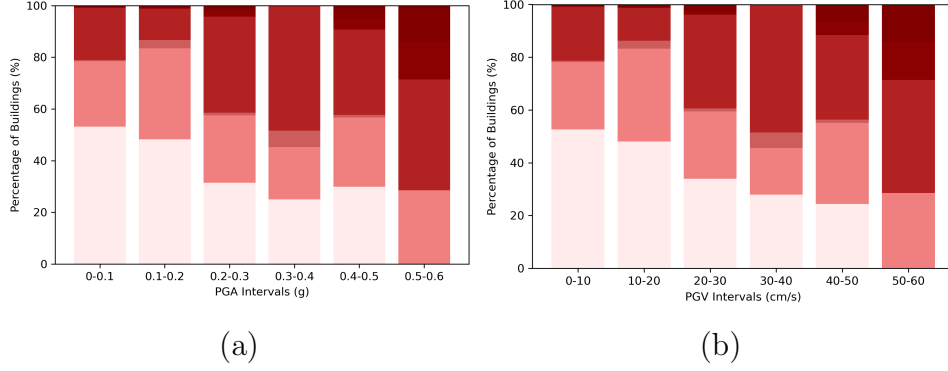


Figure 3.8. Damage states of the unreinforced masonry structures in Elazığ by (a) PGA intervals, (b) PGV intervals.

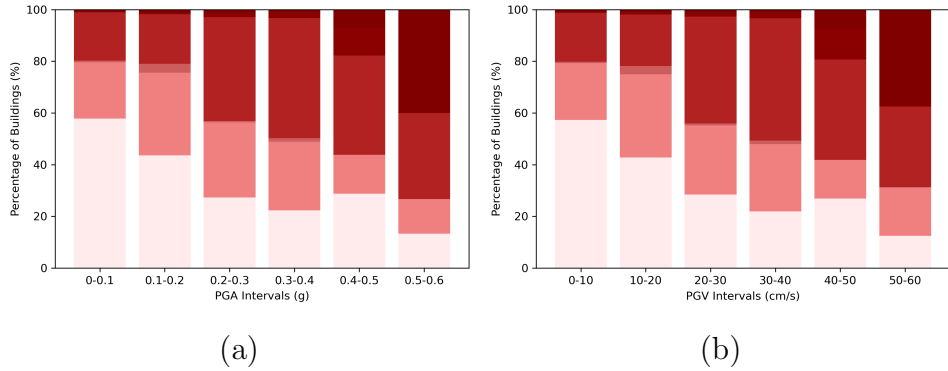


Figure 3.9. Damage states of the reinforced concrete structures in Elazığ by (a) PGA intervals, (b) PGV intervals.

The fragility curves were derived using the methodology described in Section 3.2. Also, 95% confidence intervals of the fragility curves for all damage states were found using the bootstrapping method. The estimation's degree of uncertainty is represented by the width of the confidence interval. Additionally, as stated in Porter (2007), it seems reasonable to use the same standard deviation value that is typically determined by averaging the outcomes for all damage levels as

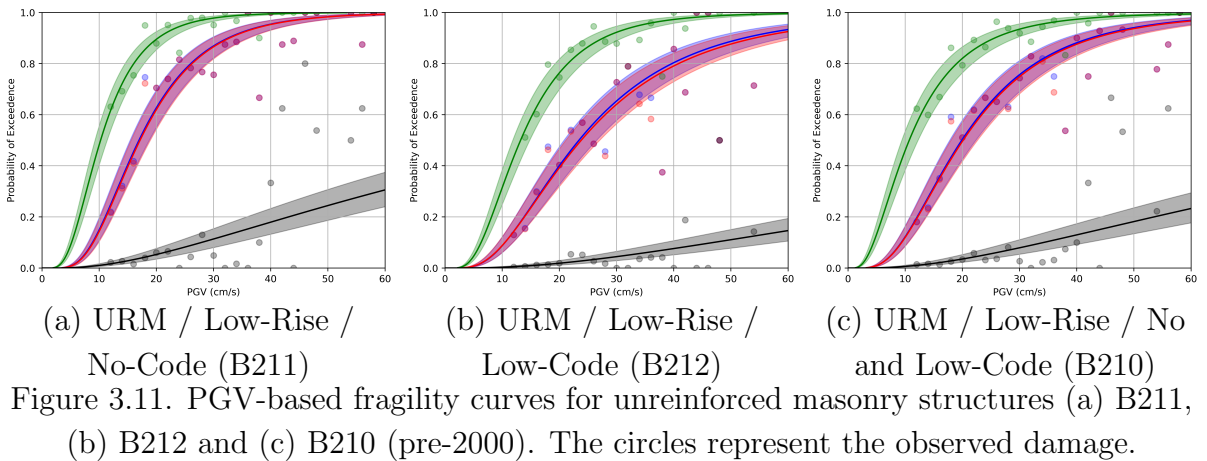
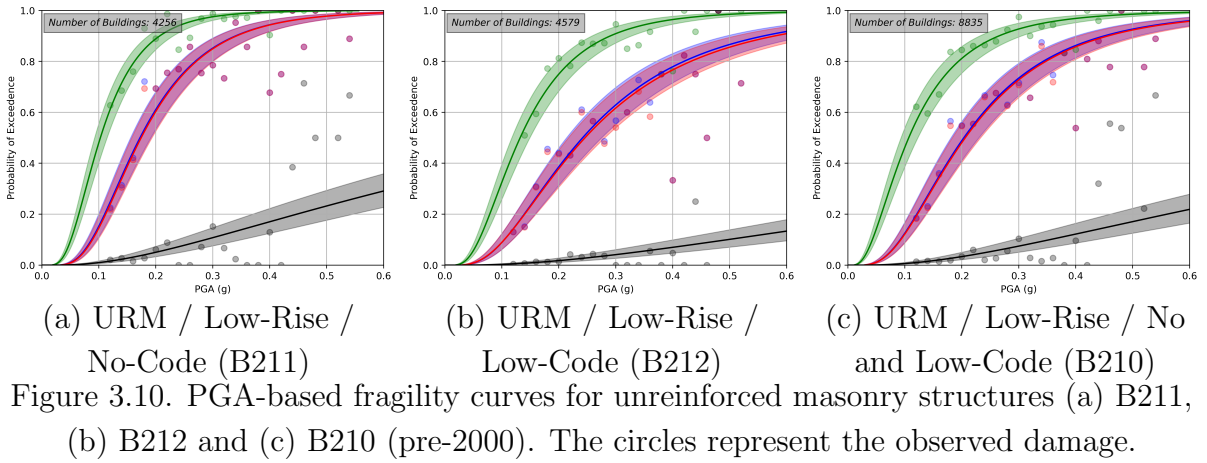
$$\beta' = \frac{1}{n} \sum_{d=1}^n \{\beta_d\} \quad (3.6)$$

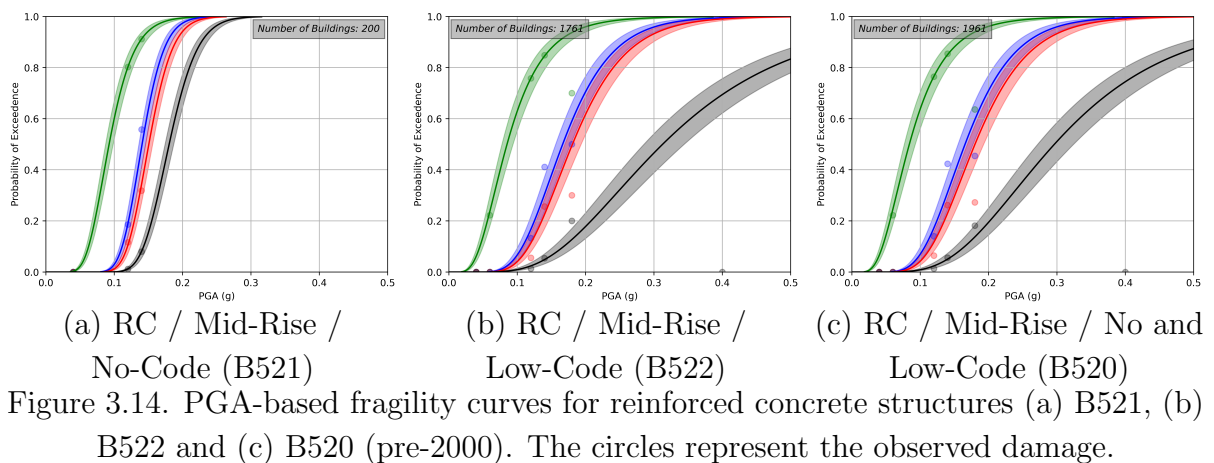
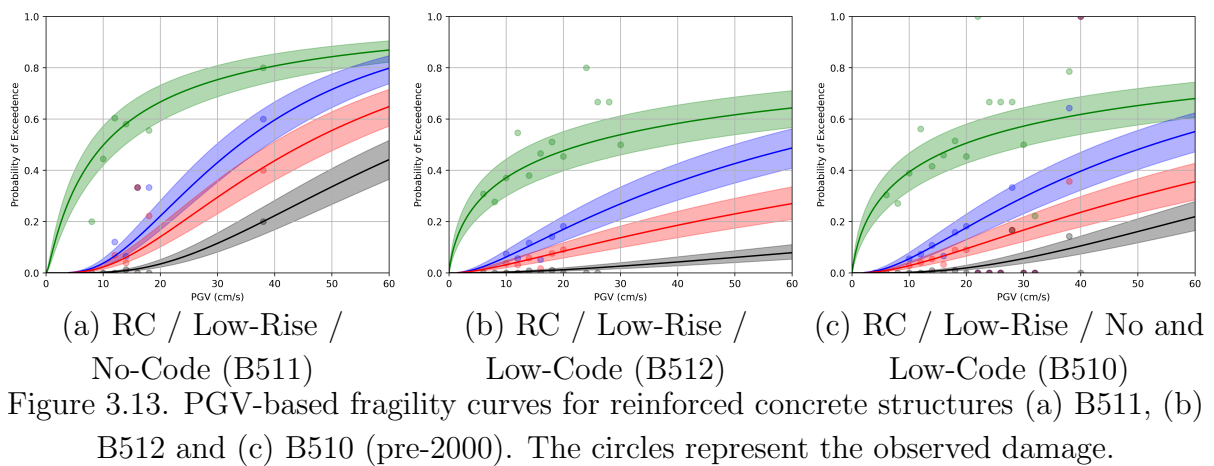
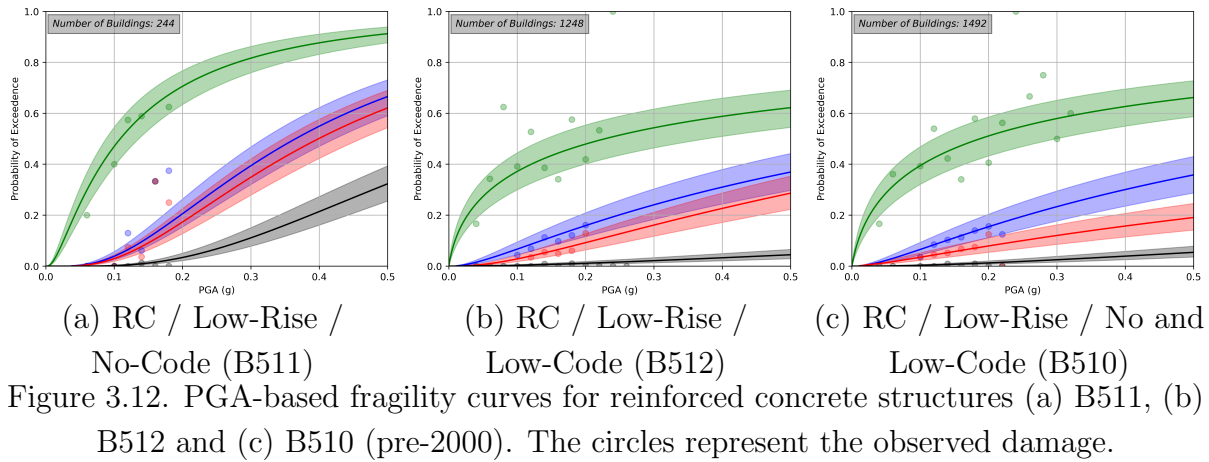
where d is damage state, n is number of considered damage states, β_d is initially derived logarithmic standard deviation of the fragility function for damage state d and

β' is the new common logarithmic standard deviation of the fragility curve that we use for all damage states. Therefore, the median value for each damage level must also be altered as

$$\theta'_d = \theta_d \times \exp(0.842 \times (\beta' - \beta_d)) \quad (3.7)$$

where θ_d is the initially derived median of the fragility function for damage state d and θ'_d is the new adjusted median value for damage state equals d . This prevents the intersection of fragility curves related to two or more damage levels [31]. Using these ground motion intensity values and the defined statistical procedures, derived fragility curves are illustrated in Figures 3.34 to 3.41 for Elazığ inventory. The cumulative log-normal distribution parameters of resulting fragility curves are given in the Appendix A.





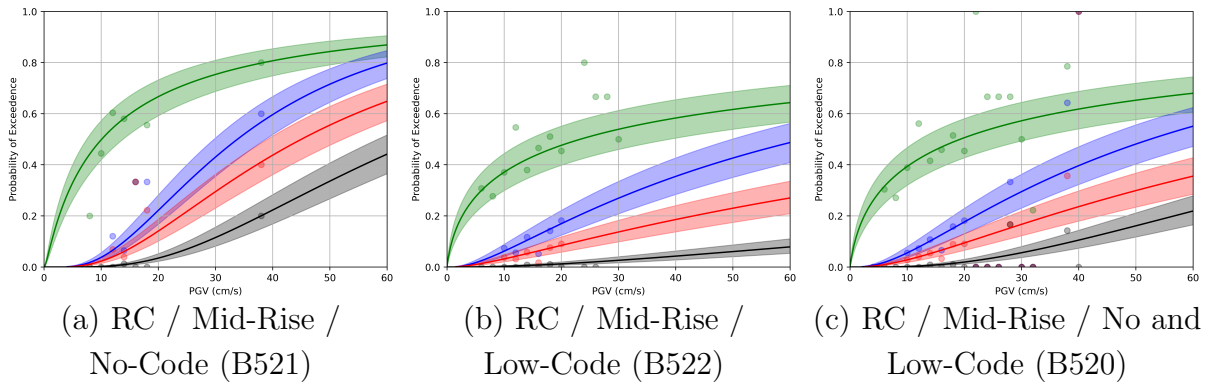


Figure 3.15. PGV-based fragility curves for reinforced concrete structures (a) B521, (b) B522 and (c) B520 (pre-2000). The circles represent the observed damage.

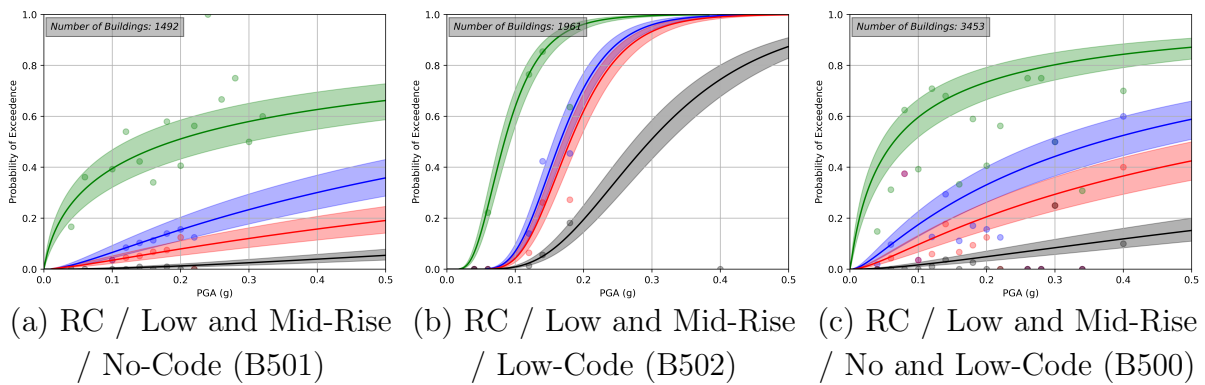


Figure 3.16. PGA-based fragility curves for reinforced concrete structures (a) B501, (b) B502 and (c) B500 (pre-2000). The circles represent the observed damage.

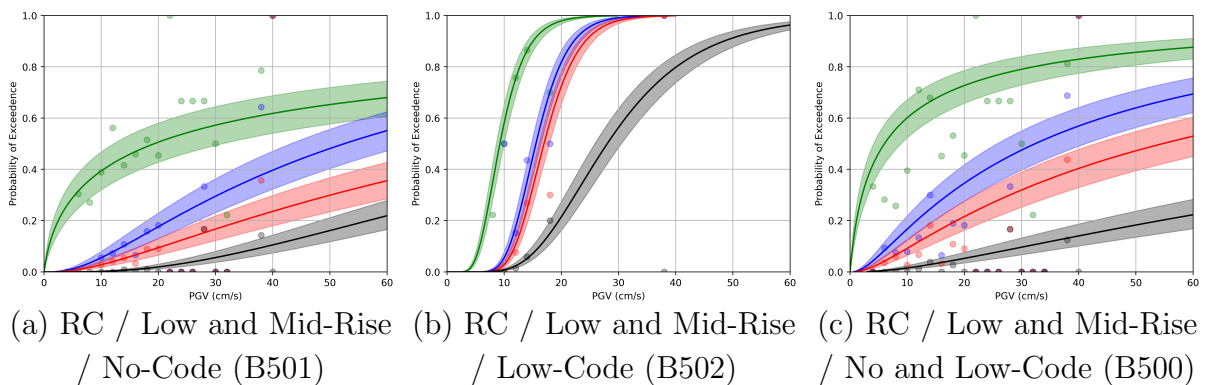


Figure 3.17. PGV-based fragility curves for reinforced concrete structures (a) B501, (b) B502 and (c) B500 (pre-2000). The circles represent the observed damage.

3.5. Comparison with Existing Fragility Curves

Empirical fragility curves may vary considerably according to the effect of the earthquake from which the data is obtained and the related building stock. For this reason, it is important to compare the obtained fragility curves with analytical and empirical fragility curves in the literature for the Turkish building stock.

Analytical fragility functions for reinforced concrete and masonry structures of Euro-Mediterranean regions (Türkiye, Greece, Italy) were produced within the scope of SYNER-G project [1]. In this project, fragility curves were created for 2, 5 and 8 story structures according to ductile and non-ductile design status. 2-story is considered low-rise and 5-story is considered mid-rise to compare the building taxonomy used in this study. The 2-story and non-ductile building class in the SYNER-G project was mapped to B511, the 2-story and ductile building class to B512, the 5-story and non-ductile building class to B521 and the 5-story and ductile building class to B522. Detailed information on building taxonomy can be found in Table 2.4. As a result, Figures 3.42 to 3.45 show the comparison of the fragility curves derived in this study with the SYNER-G project.

Akkar et al. (2005) studied PGV-based fragility curves for Turkish building stock according to the 1975 Turkish seismic code [32]. Therefore, they can be considered as low-code (constructed between 1980-2000). Their study includes 2 to 5-story reinforced concrete structures. They propose fragility curves for light, moderate and severe damage states, these damage states are compared with slight, moderate and complete damage states. In order to make a comparison, the 2-story building was matched with the low-rise class (B512) and the 5-story building type was matched with the mid-rise class (B522). Figures 3.46 and 3.47 show the comparison between fragility curves from Akkar et al. (2005) and this study [32].

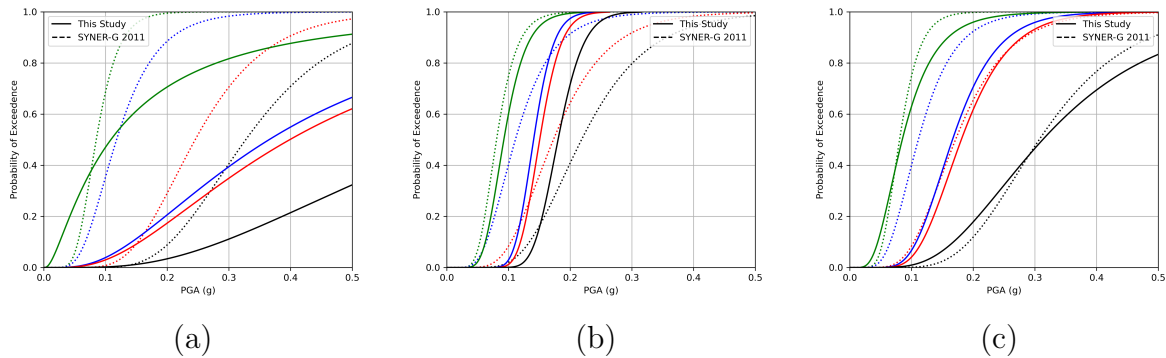


Figure 3.18. Comparison of the fragility curves for (a) 2-story, non-ductile RC MRF structures in SYNER-G project (dashed lines) with B511 building class (solid lines), (b) 5-story, non-ductile RC MRF structures in SYNER-G project with B521 building class and (c) 5-story, ductile RC MRF structures in SYNER-G project with B522 building class suggested in this study

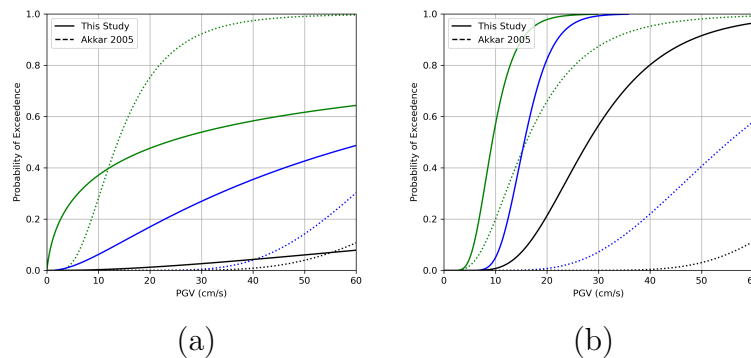


Figure 3.19. Comparison of the fragility curves for (a) 3-story RC MRF structures in Akkar et al. (2005) (dashed lines) with B512 building class (solid lines) and (b) 5-story RC MRF structures in Akkar et al. (2005) with B522 building class suggested in this study

Erberik (2008, a) derived PGV-based fragility curves for Turkish building stock that were built between 1973 and 1999 [33]. Therefore, they can be low-code or no-code (constructed before 2000). Their study includes low and mid-rise reinforced concrete structures and proposes fragility curves for serviceability, damage control, and collapse prevention damage states. These damage states are compared with slight, moderate, and complete damage states considered in this study. To make a comparison, the low-rise structures were matched with the B510 building class (low-rise, unknown construction year), and the mid-rise building type was matched with the B520 building class (mid-rise, pre-2000). In Erberik (2008, b), Fragility curves for moderate and collapse damage grades were created for urban and rural type masonry structures between 1 to 5 stories [34]. Figure 3.50 shows the comparison of fragility curves from Erberik (2008, a), Erberik (2008, b) and this study.

Gaudio et al. (2017) derived fragility curves for the Italian building stock with

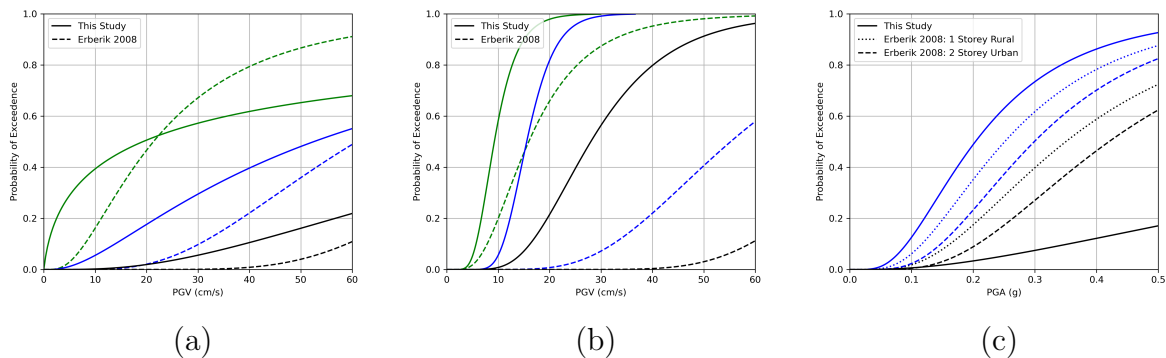


Figure 3.20. Comparison of the fragility curves for (a) low-rise RC MRF structures in Erberik (2008, a) (dashed lines) with B510 building class (solid lines), (b) mid-rise RC MRF structures in Erberik (2008, a) with B520 building class and (c) unreinforced masonry structures in Erberik (2008, b) with B520 building class suggested in this study

post-earthquake data after the 2009 L'Aquila earthquake [30]. In Gaudio et al (2017), fragility curves exist for low-rise, mid-rise and their combination for reinforced concrete structures. Since these fragility curves are independent of the year of construction, they are compared with fragility curves for which the year of construction is considered as unknown in this study. As a result, low-rise, mid-rise and their combined building classes were mapped to building classes B510, B520 and B500 respectively. Figures 3.51 to 3.53 show the comparison between fragility curves from Gaudio et al. (2017) and this study.

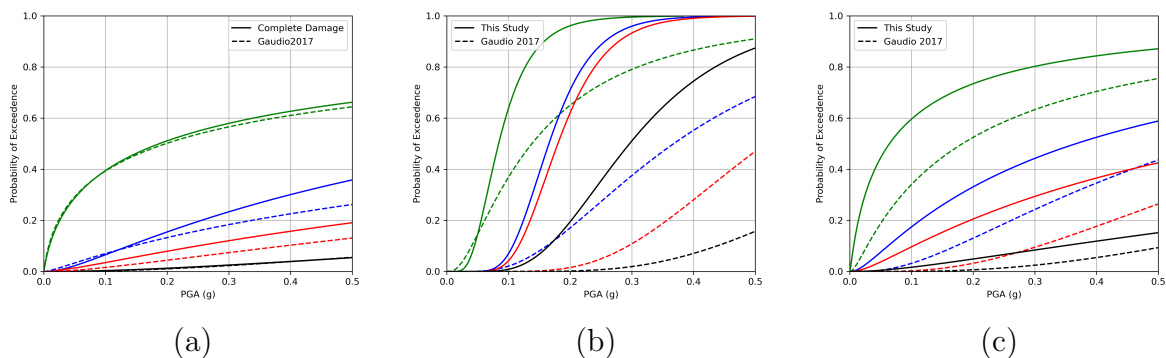


Figure 3.21. Comparison of the fragility curves for (a) low-rise RC MRF structures in Gaudio et al. (2017) (dashed lines) with B510 building class (solid lines), (b) mid-rise RC MRF structures in Gaudio et al. (2017) with B520 building class and (c) low and mid-rise RC MRF structures in Gaudio et al. (2017) with B500 building class suggested in this study

Lastly, a new European Seismic Risk Model (ESRM20) was released in the scope of the EFHER project (Crowley et al., 2021). This model consists of several types of fragility and vulnerability functions. Fragility curves for CR-LFM-CDN-H2, CR-LFM-CDN-H6 and CR-LFM-CDL-H6 building classes were mapped to building classes B511, B512 and B522 respectively. Figure 32 shows the comparison between fragility curves from Crowley et al. (2021) and this study.

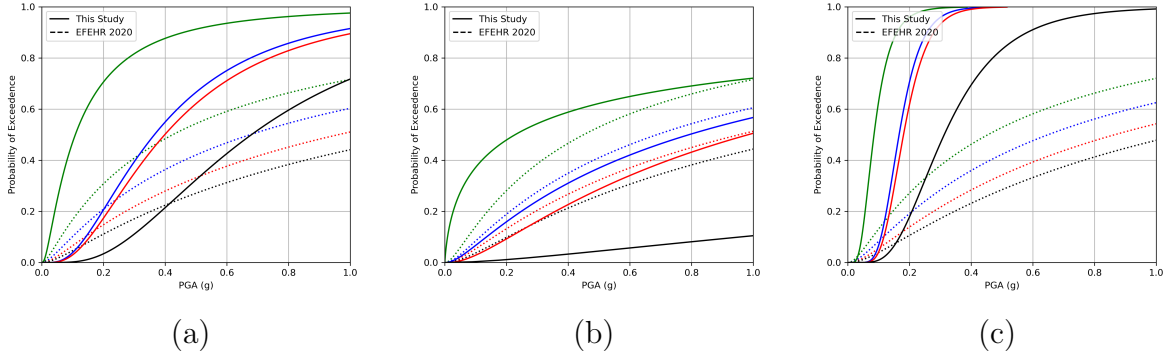


Figure 3.22. Comparison of the fragility curves for (a) CR-LFM-CDN-H2 building class in Crowley et al. (2021) (dashed lines) with B511 building class (solid lines), (b) CR-LFM-CDN-H6 building class in Crowley et al. (2021) with B512 building class and (c) CR-LFM-CDL-H6 building class in Crowley et al. (2021) with B522 building class suggested in this study

3.6. Conclusions

Türkiye experienced two significant earthquakes in 2020 that caused extensive damage. The Sivrice-Elazığ earthquake, with a moment magnitude (M_w) of 6.8, occurred on January 24, 2020 (17:55 UTC) along the East Anatolian Fault Zone. Western Türkiye and Eastern Greece were shaken by a catastrophic earthquake with a moment magnitude (M_w) of 6.6 less than a year later, on October 30, 2020 (11:51 UTC). The event left significant damage in its wake, as well as a tsunami that inundated some areas of Seferihisar (Türkiye).

After these two events, field surveys were carried out by the Turkish Ministry of Environment, Urbanization and Climate Change and the damage status of the structures in the earthquake-affected areas was determined. Damage data obtained by field surveys after major earthquakes are valuable as they enable empirical fragility curve studies. Empirical fragility curves are important because they represent the earthquake characteristics of the relevant region and the region-specific building stock, and they can be used in earthquake risk assessment studies for future earthquakes.

In this study, the building stock compiled from the field surveys conducted for Elazığ and Izmir cities are classified according to the generic building classes in Türkiye and statistics for the related cities are illustrated. The inventory statistics showed that since the damage rates are very low in the building inventory in Izmir province and the intensity measure range affecting the structures is limited, meaningful results could not be obtained despite the large number of structures (45,096) in the Izmir building inventory. In addition, statistics of Elazığ inventory showed that unreasonable results might emerge due to the low damage rate in the structures built after 2000 and the low amount of

data in the high-rise building classes. For this reason, it was decided to carry out more detailed analyses for low and medium-rise masonry and reinforced concrete structures constructed before 2000 compiled from Elazığ inventory.

Before generating final fragility curves, a sensitivity analysis was performed in Section 4 using five different ground motion models and two different V_s30 inputs in the case of unreinforced masonry structures constructed before 2000 in Elazığ (8,835 structures) to determine the effect of ground motion uncertainty on the fragility curves and to take these uncertainties into account. The study recommended using a logic tree approach to create a ground motion model rather than relying on a single model to account for the epistemic uncertainties related to ground motion models.

With the help of the findings from the previous sections, fragility functions for low and medium-rise structures built before 2000 were derived using the building inventory of Elazığ taking ground motion uncertainties into account. Furthermore, lower and upper limits corresponding to 95% confidence intervals were found for the considered fragility curves.

Finally, in Section 5, the fragility curves obtained are compared with the fragility curves applicable for Türkiye in the literature. In some of these comparisons, the obtained fragility curves and the curves for the related building class in the literature are quite similar, while the curves for some building classes are quite different from those in the literature.

3.7. Acknowledgments

The Earthquake Engineering Field Investigation Team (EEFIT) and the Institution of Structural Engineers' support through the 2022 EEFIT Research Grant Scheme is gratefully appreciated by the authors.

REFERENCES

1. Erdik, M., “Earthquake Risk Assessment”, *Bulletin of Earthquake Engineering*, Vol. 15, No. 12, pp. 5055–5092, Dec. 2017.
2. AFAD, “Disaster and Emergency Management Presidency Situation Report on January 30th, 2020”, <https://tinyurl.com/28as54k8>, accessed: 2023-8-27.
3. Erdik, M., Turkish Earthquake Foundation, M. Demircioğlu and C. Tüzün, “Forensic Analysis Reveals the Causes of Building Damage in Izmir in the Oct. 30 Aegean Sea earthquake”, *Temblor*, 2020.
4. *Applied Technology Council Report ATC-13. Earthquake Damage Evaluation Data for California*, Tech. rep., Applied Technology Council, 1985.
5. *Cahier du Centre European de Geodynamique et de Seismologie*, Tech. rep., Luxembourg, 1998.
6. *HAZUS user and technical manuals*, Tech. rep., Federal Emergency Management Agency, Washington D.C., 1999.
7. Rossetto, T. and A. Elnashai, “Derivation of Vulnerability Functions for European-type RC Structures Based on Observational Data”, *Engineering Structures.*, Vol. 25, No. 10, pp. 1241–1263, Aug. 2003.
8. *İstanbul İli Olası Deprem Kayıp Tahminlerinin Güncellenmesi Projesi*, Tech. rep., İstanbul Büyükşehir Belediyesi, 2019.
9. Maqsood, T., M. Edwards, I. Ioannou, I. Kosmidis, T. Rossetto and N. Corby, “Seismic Vulnerability Functions for Australian Buildings by Using GEM Empirical Vulnerability Assessment Guidelines”, *Natural Hazards*, Vol. 80, No. 3, pp. 1625–1650, Feb. 2016.
10. Cetin, C. and M. A. Erberik, “Kırılgnalık Egrileri Kullanılarak Elde Edilen Eahmini Hasar Dağılımının Hasar Tespit Verileriyle Karsılaştırılması”, pp. 11–13, Eskisehir, Türkiye, 2017.
11. Kircher, C. A., A. A. Nassar, O. Kustu and W. T. Holmes, “Development of Building Damage Functions for Earthquake Loss Estimation”, *Earthquake Spectra*, Vol. 13, No. 4, pp. 663–682, Nov. 1997.

12. Shinozuka, M., M. Q. Feng, J. Lee and T. Naganuma, “Statistical Analysis of Fragility Curves”, *Journal of Engineering Mechanics*, Vol. 126, No. 12, pp. 1224–1231, Dec. 2000.
13. Baker, J. W., “Efficient Analytical Fragility Function Fitting Using Dynamic Structural Analysis”, *Earthquake Spectra*, Vol. 31, No. 1, pp. 579–599, 2015.
14. Hancilar, U., K. Sesetyan and E. Cakti, “Sensitivity of the Average Annual Earthquake Loss Estimations to the Ground Motion Intensity Measure”, *17th World Conference on Earthquake Engineering*, Sendai, Japan, 2020.
15. Ioannou, I., J. Douglas and T. Rossetto, “Assessing the Impact of Ground-Motion Variability and Uncertainty on Empirical Fragility Curves”, *Soil Dynamics and Earthquake Engineering*, Vol. 69, pp. 83–92, Feb. 2015.
16. Yazgan, U., “Empirical Seismic Fragility Assessment with Explicit Modeling of Spatial Ground Motion Variability”, *Engineering Structures*, Vol. 100, pp. 479–489, Oct. 2015.
17. Lallemant, D. and A. Kiremidjian, “Accounting for Uncertainty in Earthquake Fragility Curves”, *16th World Conference on Earthquake Engineering*, 2017.
18. Ioannou, I., R. E. Chandler and T. Rossetto, “Empirical Fragility Curves: The Effect of Uncertainty in Ground Motion Intensity”, *Soil Dynamics and Earthquake Engineering*, Vol. 129, No. 105908, p. 105908, Feb. 2020.
19. Hancilar, U., C. Tuzun, C. Yenidogan and M. Erdik, “ELER Software-A New Tool for Urban Earthquake Loss Assessment”, *Natural Hazards*, Vol. 10, 2010.
20. Wald, D. J. and T. I. Allen, “Topographic Slope as a Proxy for Seismic Site Conditions and Amplification”, *Bulletin of the Seismological Society of America*, Vol. 97, No. 5, pp. 1379–1395, 10 2007.
21. Kale, Ö., “Some Discussions on Data-Driven Testing of Ground-Motion Prediction Equations Under the Turkish Ground-Motion Database”, *Journal of Earthquake Engineering*, Vol. 23, No. 1, pp. 160–181, Jan. 2019.
22. Chiou, B. S.-J. and R. R. Youngs, “Update of the Chiou and Youngs NGA Model for the Average Horizontal Component of Peak Ground Motion and Response Spectra”, *Earthquake Spectra*, Vol. 30, No. 3, pp. 1117–1153, Aug. 2014.
23. Gulerce, Z., B. Kargioglu and N. A. Abrahamson, “Turkey-Adjusted NGA-W1 Hori-

- zontal Ground Motion Prediction Models”, *Earthquake Spectra*, Vol. 32, pp. 75–100, 2016.
24. Cetin, K. O., E. Cakir, M. Ilgac, G. Can, B. Soylemez, A. Elsaid, F. Cuceoglu, Z. Gulerce, A. Askan, S. Aydin and M. Gor, “Geotechnical Aspects of Reconnaissance Findings after 2020 January 24th, M6.8 Sivrice–Elazig–Turkey Earthquake”, *Bulletin of Earthquake Engineering*, Vol. 19, No. 9, pp. 3415–3459, Jul. 2021.
 25. Abrahamson, N. A., W. J. Silva and R. Kamai, “Summary of the ASK14 Ground Motion Relation for Active Crustal Regions”, *Earthquake Spectra*, Vol. 30, No. 3, pp. 1025–1055, Aug. 2014.
 26. Askan, A., Z. Gülerce, Z. Roumelioti, D. Sotiriadis, N. S. Melis, A. Altindal, B. Akbaş, E. Sopaci, S. Karimzadeh, I. Kalogeras, N. Theodoulidis, K. Konstantinidou, A. A. Özacar, Ö. Kale and B. Margaris, “The Samos Island (Aegean Sea) M7.0 Earthquake: Analysis and Engineering Implications of Strong Motion Data”, *Bulletin of Earthquake Engineering*, Vol. 20, No. 14, pp. 7737–7762, Nov. 2022.
 27. Campbell, K. W. and Y. Bozorgnia, “NGA-West2 Ground Motion Model for the Average Horizontal Components of PGA, PGV, and 5% Damped Linear Acceleration Response Spectra”, *Earthquake Spectra*, Vol. 30, No. 3, pp. 1087–1115, Aug. 2014.
 28. Akkar, S., M. A. Sandikkaya and J. J. Bommer, “Empirical Ground-Motion Models for Point- and Extended-Source Crustal Earthquake Scenarios in Europe and the Middle East”, *Bulletin of Earthquake Engineering*, Vol. 12, No. 1, pp. 359–387, Feb. 2014.
 29. Boore, D. M., J. P. Stewart, E. Seyhan and G. M. Atkinson, “NGA-West2 Equations for Predicting PGA, PGV, and 5% Damped PSA for Shallow Crustal Earthquakes”, *Earthquake Spectra*, Vol. 30, No. 3, pp. 1057–1085, Aug. 2014.
 30. Del Gaudio, C., G. De Martino, M. Di Ludovico, G. Manfredi, A. Prota, P. Ricci and G. M. Verderame, “Empirical fragility curves from damage data on RC buildings after the 2009 L’Aquila earthquake”, *Bull. Earthquake Eng.*, Vol. 15, No. 4, pp. 1425–1450, Apr. 2017.
 31. Porter, K., “A beginner’s Guide to Fragility, Vulnerability, and Risk”, *Encyclopedia of Earthquake Engineering*, pp. 1–29, Berlin, Heidelberg, 2021.
 32. Akkar, S., H. Sucuoglu and A. Yakut, “Displacement-Based Fragility Functions for Low- and Mid-Rise Ordinary Concrete Structures”, *Earthquake Spectra*, Vol. 21, pp. 901–927, 2005.

33. Erberik, M. A., “Fragility-based Assessment of Typical Mid-Rise and Low-Rise RC Structures in Turkey”, *Engineering Structures*, Vol. 30, pp. 1360–1374, 2008.
34. Erberik, M. A., “Generation of Fragility Curves for Turkish Masonry Structures Considering in-plane Failure Modes”, *Earthquake Engineering and Structural Dynamics*, Vol. 37, pp. 387–405, 2008.

APPENDIX A: FRAGILITY CURVE PARAMETERS

In this appendix, the cumulative log-normal distribution parameters of resulting fragility curves which are shown in Chapter 3.5 are given. In the tables, the median and standard deviation are given along with the upper and lower bounds of the 95% confidence intervals in parentheses.

Table A.1. PGA-based fragility curve parameters for building class B211.

Damage State	Median	Standard Deviation
Slight	(0.093) 0.103 (0.115)	0.547
Moderate	(0.156) 0.172 (0.192)	0.531
Extensive	(0.158) 0.174 (0.194)	0.526
Complete	(0.865) 1.044 (1.277)	1.007

Table A.2. PGA-based fragility curve parameters for building class B212.

Damage State	Median	Standard Deviation
Slight	(0.118) 0.132 (0.149)	0.615
Moderate	(0.214) 0.242 (0.276)	0.655
Extensive	(0.217) 0.246 (0.281)	0.669
Complete	(1.663) 2.045 (2.549)	1.105

Table A.3. PGA-based fragility curve parameters for building class B210.

Damage State	Median	Standard Deviation
Slight	(0.094) 0.107 (0.123)	0.709
Moderate	(0.181) 0.204 (0.23)	0.619
Extensive	(0.183) 0.206 (0.233)	0.621
Complete	(1.106) 1.344 (1.653)	1.039

Table A.4. PGV-based fragility curve parameters for building class B211.

Damage State	Median	Standard Deviation
Slight	(9.271) 10.246 (11.396)	0.534
Moderate	(15.421) 16.964 (18.775)	0.509
Extensive	(15.59) 17.141 (18.963)	0.506
Complete	(82.431) 99.245 (120.921)	0.99

Table A.5. PGV-based fragility curve parameters for building class B212.

Damage State	Median	Standard Deviation
Slight	(11.865) 13.219 (14.831)	0.577
Moderate	(20.831) 23.428 (26.548)	0.627
Extensive	(21.129) 23.826 (27.075)	0.641
Complete	(150.972) 184.405 (228.156)	1.067

Table A.6. PGV-based fragility curve parameters for building class B210.

Damage State	Median	Standard Deviation
Slight	(9.427) 10.711 (12.271)	0.681
Moderate	(17.809) 19.895 (22.384)	0.591
Extensive	(18.008) 20.133 (22.669)	0.595
Complete	(104.084) 125.928 (154.234)	1.016

Table A.7. PGA-based fragility curve parameters for building class B511.

Damage State	Median	Standard Deviation
Slight	(0.088) 0.109 (0.136)	1.124
Moderate	(0.318) 0.365 (0.422)	0.733
Extensive	(0.348) 0.399 (0.462)	0.733
Complete	(0.6) 0.68 (0.777)	0.67

Table A.8. PGA-based fragility curve parameters for building class B512.

Damage State	Median	Standard Deviation
Slight	(0.142) 0.228 (0.377)	2.521
Moderate	(0.612) 0.792 (1.043)	1.379
Extensive	(0.786) 0.984 (1.25)	1.2
Complete	(5.289) 7.085 (9.672)	1.56

Table A.9. PGA-based fragility curve parameters for building class B510.

Damage State	Median	Standard Deviation
Slight	(0.121) 0.187 (0.299)	2.348
Moderate	(0.64) 0.832 (1.101)	1.403
Extensive	(1.622) 2.236 (3.147)	1.712
Complete	(3.89) 5.102 (6.807)	1.446

Table A.10. PGV-based fragility curve parameters for building class B511.

Damage State	Median	Standard Deviation
Slight	(7.492) 10.091 (13.853)	1.588
Moderate	(29.75) 33.833 (38.797)	0.686
Extensive	(39.091) 45.021 (52.322)	0.753
Complete	(58.414) 66.094 (75.38)	0.659

Table A.11. PGV-based fragility curve parameters for building class B512.

Damage State	Median	Standard Deviation
Slight	(14.396) 23.32 (38.965)	2.573
Moderate	(49.889) 62.352 (79.054)	1.19
Extensive	(110.563) 144.81 (192.983)	1.44
Complete	(302.08) 386.726 (503.013)	1.318

Table A.12. PGV-based fragility curve parameters for building class B510.

Damage State	Median	Standard Deviation
Slight	(12.23) 19.282 (31.301)	2.429
Moderate	(43.226) 52.517 (64.608)	1.039
Extensive	(74.221) 92.302 (116.408)	1.163
Complete	(98.849) 115.912 (137.318)	0.85

Table A.13. PGA-based fragility curve parameters for building class B521.

Damage State	Median	Standard Deviation
Slight	(0.121) 0.111 (0.299)	1.727
Moderate	(0.64) 1.094 (1.101)	1.727
Extensive	(1.622) 2.265 (3.147)	1.727
Complete	(3.89) 6.465 (6.807)	1.727

Table A.14. PGA-based fragility curve parameters for building class B522.

Damage State	Median	Standard Deviation
Slight	(0.078) 0.085 (0.094)	0.49
Moderate	(0.157) 0.167 (0.179)	0.339
Extensive	(0.17) 0.181 (0.194)	0.339
Complete	(0.286) 0.313 (0.345)	0.485

Table A.15. PGA-based fragility curve parameters for building class B520.

Damage State	Median	Standard Deviation
Slight	(0.077) 0.084 (0.093)	0.491
Moderate	(0.155) 0.166 (0.177)	0.341
Extensive	(0.169) 0.18 (0.193)	0.341
Complete	(0.272) 0.296 (0.324)	0.456

Table A.16. PGV-based fragility curve parameters for building class B521.

Damage State	Median	Standard Deviation
Slight	(8.883) 9.369 (9.916)	0.284
Moderate	(13.593) 14.18 (14.831)	0.225
Extensive	(14.69) 15.323 (16.027)	0.225
Complete	(22.374) 23.967 (25.787)	0.367

Table A.17. PGV-based fragility curve parameters for building class B522.

Damage State	Median	Standard Deviation
Slight	(8.735) 9.373 (10.102)	0.376
Moderate	(14.821) 15.588 (16.447)	0.269
Extensive	(16.115) 16.949 (17.884)	0.269
Complete	(25.858) 27.988 (30.446)	0.422

Table A.18. PGV-based fragility curve parameters for building class B520.

Damage State	Median	Standard Deviation
Slight	(8.62) 9.255 (9.982)	0.379
Moderate	(14.765) 15.553 (16.437)	0.277
Extensive	(16.101) 16.96 (17.925)	0.277
Complete	(25.865) 28.02 (30.51)	0.427

Table A.19. PGA-based fragility curve parameters for building class B501.

Damage State	Median	Standard Deviation
Slight	(0.057) 0.071 (0.09)	1.155
Moderate	(0.184) 0.205 (0.23)	0.573
Extensive	(0.25) 0.283 (0.324)	0.676
Complete	(0.381) 0.426 (0.48)	0.597

Table A.20. PGA-based fragility curve parameters for building class B502.

Damage State	Median	Standard Deviation
Slight	(0.047) 0.066 (0.095)	1.837
Moderate	(0.302) 0.401 (0.542)	1.513
Extensive	(0.553) 0.74 (1.009)	1.554
Complete	(2.431) 3.32 (4.625)	1.662

Table A.21. PGA-based fragility curve parameters for building class B500.

Damage State	Median	Standard Deviation
Slight	(0.046) 0.064 (0.092)	1.81
Moderate	(0.283) 0.367 (0.484)	1.386
Extensive	(0.501) 0.657 (0.876)	1.444
Complete	(1.706) 2.243 (3.001)	1.459

Table A.22. PGV-based fragility curve parameters for building class B501.

Damage State	Median	Standard Deviation
Slight	(2.892) 4.285 (6.511)	2.097
Moderate	(25.936) 31.977 (39.959)	1.117
Extensive	(34.81) 42.918 (53.631)	1.117
Complete	(62.116) 88.886 (87.652)	1.117

Table A.23. PGV-based fragility curve parameters for building class B502.

Damage State	Median	Standard Deviation
Slight	(4.31) 6.26 (9.313)	1.991
Moderate	(26.999) 34.47 (44.705)	1.303
Extensive	(45.667) 58.73 (76.761)	1.342
Complete	(148.052) 191.589 (252.07)	1.375

Table A.24. PGV-based fragility curve parameters for building class B500.

Damage State	Median	Standard Deviation
Slight	(4.152) 6.027 (8.96)	1.988
Moderate	(25.789) 32.387 (41.271)	1.215
Extensive	(43.004) 54.633 (70.484)	1.277
Complete	(125.46) 159.543 (206.043)	1.282